AD NUMBER

AD050212

NEW LIMITATION CHANGE

TO

Approved for public release, distribution unlimited

FROM

Distribution authorized to U.S. Gov't. agencies and their contractors; Administrative/Operational Use; JUN 1954. Other requests shall be referred to Wright Air Development Center, Wright-Patterson AFB, OH 45433.

AUTHORITY

AFAL ltr, 17 Aug 1979

WADC TECHNICAL REPORT 54-29

THEORETICAL STUDIES OF THE EFFECTS OF ASPECT RATIO ON FLUTTER

MARTIN GOLAND
Y. L. LUKE
M. A. DENGLER

MIDWEST RESEARCH INSTITUTE

JUNE 1954

WRIGHT AIR DEVELOPMENT CENTER

WADC TECHNICAL REPORT 54-29

THEORETICAL STUDIES OF THE EFFECTS OF ASPECT RATIO ON FLUTTER

Martin Goland
Y. L. Luke
M. A. Dengler

Midwest Research Institute

June 1954

Aircraft Laboratory
Contract No. AF18(600)-129
Contract No. AF33(038)-10400
RDO No. 459-36

Wright Air Development Center
Air Research And Development Command
United States Air Force
Wright-Patterson Air Force Base, Ohio

Carpenter Litho & Prtg. Co., Springfield, Ohio
20 - 16 September 1954

FOREWORD

The research described in this report was conducted by the Midwest Research Institute, Kansas City, Missouri, under U. S. Air Force Contracts AF 33(038)-10400 and AF 18(600)-129. This project was initiated by the Aircraft Laboratory, Wright Air Development Center, and was administered by Major R. L. Ely, Lt. M. Epstein and Mr. I. H. Spielberg of the Dynamics Branch of the Aircraft Laboratory. The work on these contracts was authorized by Research and Development Order No. 459-36, "Research and Investigation of Flutter".

ABSTRACT

Subsonic flutter calculations on the basis of a variety of aerodynamic theories are presented for nine model wings. The aerodynamic theories employed include two-dimensional strip theory, two variants of a procedure suggested by Wasserman (Ref. 1), the single-lifting-line theory, and the double-lifting-line theory. All save the first include corrections for the effects of finite span.

Experimental flutter speed and frequency data are available for all nine wings. The wings are of the uniform variety, have moderate to large aspect ratios, and range in sweepback from 0° to 45°. Both semi-rigid and elastic cantilever wing models are included.

A comparison of the calculated and experimental flutter speeds leads to the conclusion that two-dimensional strip theory should presently be used in the design office for the flutter analysis of unswept, or slightly swept wings. For sharply swept wings, the studies indicate that the single-lifting-line theory holds most promise for accurate flutter speed prediction. None of the theories appear to predict the flutter frequencies with satisfactory consistency.

In addition to a description of the numerous flutter calculations, the report contains an outline of the single-and double-lifting-line theories, and of the Wasserman method. The former two aerodynamic treatments were developed during the course of the present program and are efforts to devise a rational, finite span theory for the oscillating wing.

PUBLICATION REVIEW

This report has been reviewed and is approved.

FOR THE COMMANDER:

for Daniel D. McKee
Colonel, USAF
Chief, Aircraft Laboratory
Directorate of Laboratories

CONTENTS

LIST OF TABLES

LIST OF ILLUSTRATIONS

TABLE OF SYMBOLS

a_o, a_1	= see Eq. (2.11).
AR	= aspect ratio of wing model plus image.
A(gb,b), B(gb,b)	= integrals related to the incomplete Cicala function. See Eq. (II.12)..
b	= local wing semi-chord, measured parallel to direction of flow. Also used in a general discussion in Appendix II to designate either b_1 or b_2.
b_1, b_2	= see Eq. (II.9).
b_r	= wing semi-chord at reference station.
B = B(y), bA = bA(y)	= spanwise variation of the wing pitching amplitude and plunging amplitude at the forward quarter-chord line, respectively.
c_1, c_2, c_3	= see Eq. (2.38).
C(k) = F(k)+iG(k)	= Theodorsen circulation function.
C_{L_α}	= wing lift coefficient slope.
D(g,b)	= see Eq. (II.10).
d	= distance elastic axis lies to the rear of the quarter-chord divided by semi-chord.
e	= superscript employed with notation for downwash to designate that downwash is effective.
F,G	= real and imaginary parts of circulation function, respectively. A subscript 3 refers to three-dimensional flow.
F(b), F(kζ)	= the complete Cicala function, see Eqs. (II.5, 11). The real and imaginary parts are notated F_R and F_I, respectively.

g	= superscript employed with notation for downwash to designate that downwash is geometric. Also used in place of g_1 or g_2.
g_1, g_2	= see Eq. (II.9).
$g^{(p)}$, $g^{(q)}$	= damping factor in wing bending and torsion mode, respectively.
$G(u)$	= see Eq. (2.37).
$\bar{G}(b)$	= see Eq. (II.11).
$H_0^{(2)}$, $H_1^{(2)}$	= Hankel functions of second kind and order zero and one, respectively.
$H(k\zeta)$	= see Eq. (II.6).
I	= wing mass moment of inertia per unit span about elastic axis.
i	= imaginary unit.
k	= reduced frequency = $\omega b/V$.
$\bar{k}$	= see Eq. (II.9).
M	= Mach No.
$L, M_{c/4}$	= wing lift and nose-up moment about the forward quarter-chord point, each per unit span, respectively.
m	= mass of wing per unit span.
n	= letter used to designate number of horseshoe vortices.
$n=n(k)$; $\bar{n}=\bar{n}(k, w_1^{(g)}/w_2^{(g)})$	= bound vorticity correction factor used in single-lifting-line and double-lifting-line theory, respectively.
P_o, P_1, P_o, P_1, $\bar{P}_o$, $\bar{P}_1$	= see Eq. (2.7), (2.9) and (2.10).
p, q	= subscripts and superscripts used to denote items relating to wing bending and wing torsion degrees of freedom.

r	= subscript designating a vortex.
$R_1(x)$, $R_2(x)$	= see Eq. (II.2).
s	= wing semi-span measured normal to direction of flow. Also a subscript denoting a point at which downwash is satisfied.
S	= wing mass static unbalance per unit span, positive if center of gravity lies aft of the elastic axis.
t	= time coordinate.
u, v	= see Eq. (II.9).
V	= main stream velocity.
V_{exp}, V_{th}	= experimental and calculated flutter speed, respectively.
V_c	= wing speed corrected for Mach No. and used in V-g diagrams.
$(V/b\omega)_{exp}$, $(V/b\omega)_{th}$	= experimental and calculated reduced flutter velocity, respectively.
$V\,w_{rs}$	= aerodynamic influence coefficient relating the intensity of the $r^{\underline{th}}$ vortex to the downwash at the $s^{\underline{th}}$ downwash satisfaction point. For precise definitions of $V\,w_{rs}^{(11)}$, $V\,w_{rs}^{(12)}$, etc., see p. 20.
$w^{(e)}$, $w^{(g)}$	= effective and geometric downwash, respectively.
$w^{(i)}$	= finite aspect ratio induction downwash.
$w_1^{(e)}$, $w_2^{(e)}$	= effective downwash at rear quarter-chord point and mid-chord point, respectively.
$w_1^{(g)}$, $w_2^{(g)}$	= geometric downwash at mid-chord point and rear quarter-chord point, respectively.
$w_s^{(g)}$, $w_s^{(t)}$	= geometric and theoretical downwash of the wing at point s, respectively.

w_{1r}, w_{2r} = downwash velocities due to γ_r wake only at mid-chord and rear quarter-chord, respectively. A superscript e or g means that downwash is effective or geometric, respectively.

w_{rs}, $\bar{w}_{rs}$ = downwash influence coefficient relating the intensity of the $r^{\underline{th}}$ vortex to the downwash at the $s^{\underline{th}}$ downwash satisfaction point.

$w_{1s}^{(g)}$, $w_{2s}^{(g)}$ = geometric downwash of wing at 1/2 chord line and 3/4 chord line, respectively, each at station s.

w_i = induced downwash on the wing at the root.

w_{iP} = induced downwash at root arising from intensity Γ of horseshoe vortex.

$\bar{w}$, $\bar{w}_b$, $\bar{w}_w$ = see Eq. (II.1).

x = rearward coordinate in the stream direction.

$\bar{x}$ = non-dimensional rearward coordinate with origin at mid-chord.

x_{rs} = distance the point s lies behind the vortex Γ_r (in the stream direction).

y = spanwise coordinate, positive to the right.

y_{rs} = distance the point s lies to the right of the mid-span of vortex Γ_r.

z = downwash displacement of the wing.

α = wing angle of attack.

γ = Eulerian constant (see Appendix II).

γ, $\bar{\gamma}$ = circulation at a spanwise station assuming three-dimensional and two-dimensional flow, respectively.

$\bar{\gamma}_r$ = two-dimensional circulation at reference station.

$\Gamma(y)$ = spanwise distribution of the bound vorticity.

Γ_1, Γ_2 = intensities of discrete vortices γ_1 and γ_2, respectively, used in two-lifting-line theory, e.g. $\Gamma_1 = \gamma_1 b V$.

$\Gamma_r e^{i\omega t}$ = intensity of bound vorticity of r^{th} vortex.

δ = distance from the bound vortex mid-span rearward to the wing trailing edge divided by the local semi-chord.

η = semi-span of a horseshoe vortex.

λ = dummy variable of integration.

$\mu(k)$ = see Eq. (2.36).

ω = circular frequency of wing oscillation.

$\omega_{exp}, \omega_{th}$ = experimental and calculated flutter frequency, respectively.

ω_p, ω_q = circular frequency of wing bending and torsion mode, respectively.

$\Pi(x)$ = chordwise pressure distribution.

ρ = mass air density.

$\bar{\theta}, \theta$ = a parameter defined by $\bar{x} = -\cos\bar{\theta}$. Also a phase angle.

φ = angle of sweep.

ξ = rearward coordinate denoting distance from quarter-chord. Also used to denote distance behind the trailing edge.

ξ_1, ξ_2 = location of discrete vortices γ_1, γ_2 used in two-lifting-line theory.

ξ', ξ'' = rearward coordinates with origins at discrete vortices γ_1 and γ_2, respectively.

ζ = see Eq. (II.5).

INTRODUCTION

1. As its original objective, this program aimed toward an evaluation of the accuracy of a method proposed by L. S. Wasserman for accounting for finite aspect-ratio effects in flutter calculations. However, as the program progressed, certain original aerodynamic contributions were made by the authors, in the form of one-lifting-line and two-lifting-line theories for calculation of the loading of oscillating airfoils, and this work was incorporated in the over-all scope of the project.

This report describes the application of these aerodynamic theories to nine wing flutter models, for which experimental flutter data are available for comparison with the theoretical predictions. Because of the program history, all nine wings were not analyzed by all the theories; however, sufficient calculations were performed to permit preliminary appaisal of the accuracies of the various proposed design techniques.

2. The nine wings selected for analysis all were to flutter in a fundamental wing bending - fundamental wing torsion mode, and none of the models were equipped with control surfaces. The reasons for this selection are evident: To begin with, additional refinements must be introduced in the aerodynamic analysis to permit treatment of wings with discontinuous camber, as are introduced by conventional control surfaces. Although the direction of such refinements is known, the additional increase in computational complexity is hardly warranted for this preliminary appraisal of the theories.

Secondly, the comparison of calculated and measured flutter speeds can be used as an index of the excellence of a particular aerodynamic theory only if the elastic, inertia, and damping properties of the wings are known with considerable accuracy. Least difficulties in these phases of the calculation are encountered when fundamental bending - fundamental torsion flutter modes are employed. In this connection, care was exercised to insure that the higher wing bending and torsion modes were well separated from the fundamental pair; for wing No. 9, however, this requirement was not met, the wing being tested after the calculations were started.

3. In the later sections of the report, a description of the Midwest Research Institute aerodynamic theories is given. An outline of the Wasserman method, essentially following his original presentation (see Ref. 1), is also included as Appendix I. The various flutter analyses are then described in detail, and preliminary design conclusions and recommendations are drawn.

As an additional aid in appraising the merits of the finite-span theories, flutter calculations were also performed by conventional "strip" theory, employing the two-dimensional air forces, as described in Refs. 2 and 13. Conclusions are presented regarding the suitability of using two-dimensional strip theory analyses in practice.

I. METHODS FOR CALCULATION OF THE AERODYNAMIC LOADING ON OSCILLATING AIRFOILS BY LIFTING-LINE TECHNIQUES

A. Single-Lifting-Line Model

1. The theoretical basis for the single lifting-line technique for calculating the aerodynamic loading on an oscillating airfoil is described in detail in a recent research paper (see Ref. 4). In essence, the reasoning is based on extension to the oscillatory case of the ideas employed by Weissinger when analyzing steady-state wing loading.

The principal elements of the theory are as follows:

a) It is assumed that the chordwise pressure distribution at each wing station remains essentially the same as that encountered in two-dimensional flow. Thus, the local center-of-pressure is at the forward quarter-chord point of each wing station.

b) To calculate the spanwise distribution of wing circulation, the actual wing is first replaced by a concentrated line vortex which runs along the forward quarter-chord line of the wing. For a wing station where the actual bound circulation is $\Gamma e^{i\omega t}$ and the local reduced frequency is k, the line vortex is arbitrarily assigned an intensity $ne^{i(3/2)k}\Gamma e^{i\omega t}$.

Here $ne^{i(3/2)k}$ is a factor which causes the circulation prediction from the present single-lifting-line theory to correspond precisely with that from the exact, Theodorsen theory for the oscillating wing of infinite aspect ratio. The factor $n = n(k)$ is a function of the local reduced frequency only, and is given in tabular and plot form in Table I and Fig. 1, respectively.

c) With the bound vorticity accounted for, it is now necessary to construct the associated wake. This is done in the following fashion: The wake intensity at a point behind the actual wing is deduced on the basis of the exact, surface-loading theory for an oscillating airfoil (see, for example, Refs. 5, 6). This fixes the wake intensity at each point behind the trailing edge of a particular station, and located a distance ξ from the local quarter-chord of the station.

TABLE I

VALUES OF THE FUNCTION n(k) FOR VARIOUS k
(SINGLE-LIFTING-LINE THEORY)

$$n(k) = e^{-ik/2}(\pi k/2)\left[H_0^{(2)}(k) - iH_1^{(2)}(k)\right] + ike^{-ik}\left[i\pi/2 + iSi(k) + Ci(k)\right]$$

k	n(k)
0	1.0
0.05	0.9995 + 0.00961
0.10	0.9980 + 0.01911
0.15	0.9951 + 0.02841
0.20	0.9905 + 0.03761
0.30	0.9771 + 0.05641
0.40	0.9554 + 0.07721
0.50	0.9250 + 0.10241
0.60	0.8854 + 0.13501
0.80	0.7816 + 0.23581
1.00	0.6579 + 0.40731

TABLE I

VALUES OF THE FUNCTION n(k) FOR VARIOUS k
(SUBSONIC-LIFTING-LINE THEORY)

$$n(k) = e^{-ik/2}(\pi k/2)\left[H_0^{(2)}(k) - iH_1^{(2)}(k)\right] + ike^{-ik}\left[i\pi/2 + iSi(k) + Ci(k)\right]$$

k	n(k)
0	1.0
0.05	0.9995 + 0.00961
0.10	0.9980 + 0.01911
0.15	0.9951 + 0.02841
0.20	0.9905 + 0.03761
0.30	0.9771 + 0.05641
0.40	0.9554 + 0.07721
0.50	0.9250 + 0.10241
0.60	0.8854 + 0.13501
0.80	0.7816 + 0.23581
1.00	0.6579 + 0.40731

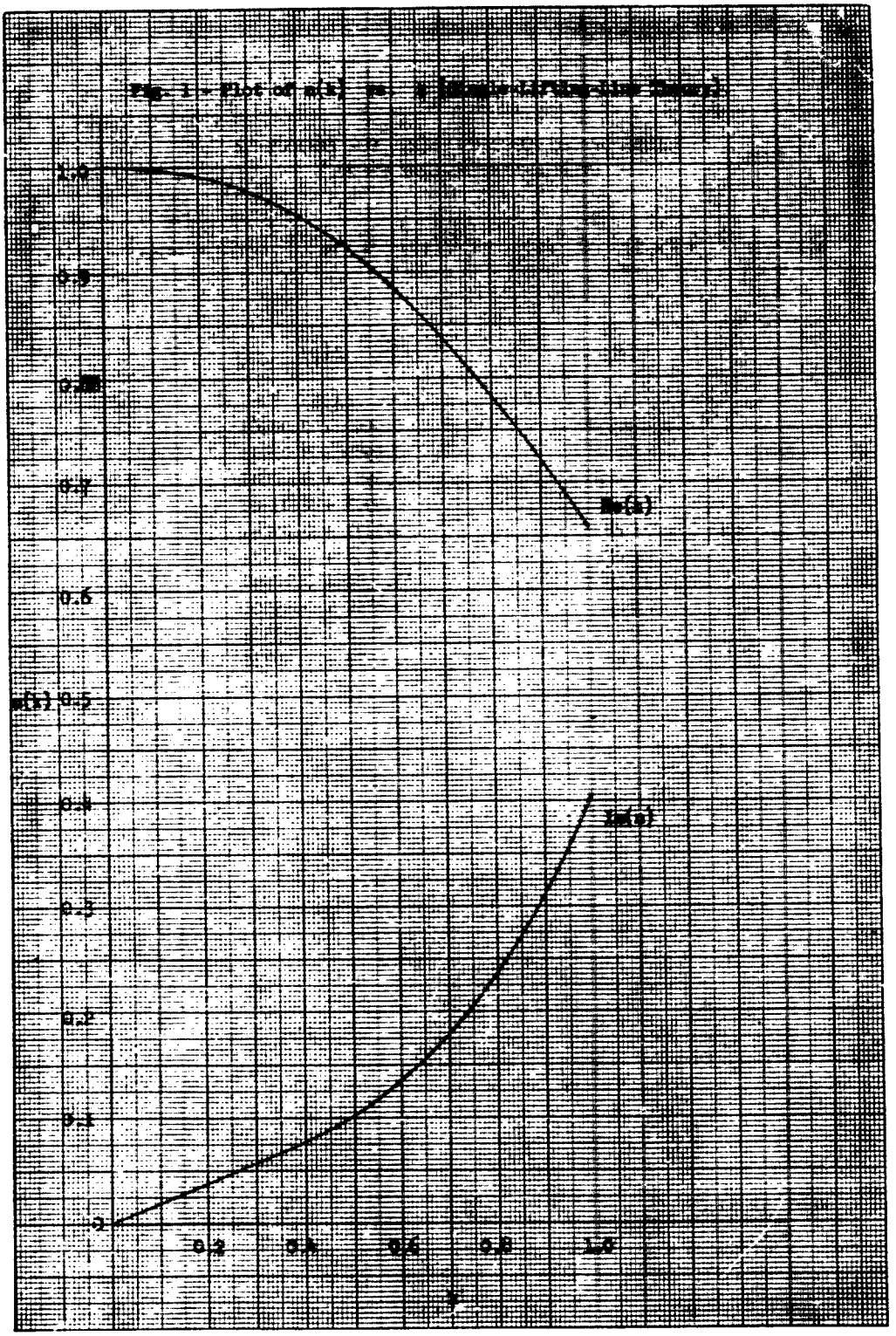

Fig. 1 - Plot of m(x) vs. x [illegible]

Now, for the single-lifting-line wing model, the wake intensity at a distance ξ behind the bound vortex is kept at precisely the same value as in the corresponding location of the actual wing. Thus if, $\underline{W}(\xi)$ is the vector wake intensity of the actual wing, and $\underline{W}^*(\xi)$ is that for the model, $\underline{W}(\xi) = \underline{W}^*(\xi)$.

Finally, for computational convenience, the lifting-line model wake is not started at the trailing edge location, but is instead arbitrarily extended forward to the bound vortex itself. In the stream direction, the wake oscillates with frequency k; this oscillatory character is simply continued forward in the region between the quarter-chord location and that of the trailing edge.

It should be particularly noted that the wake intensity behind a given wing station depends only on the value of the bound circulation at that station, and is not dependent on the bound circulation at other wing stations. The wake construction is thus simple and direct.

d) With the bound and wake vorticities thus defined, it is evident that the total downwash at any point on the actual wing planform can be formally calculated in a straightforward manner. For the single-lifting-line theory, this is done along the rear quarter-chord line of the actual wing planform. For a given wing geometry, and for a given oscillation frequency ω and air speed V, the downwash at a particular point on this line depends on the function $\Gamma(y)$, i.e., on the spanwise distribution of the bound vorticity.

For the single-lifting-line theory, it is proposed that the total velocity calculated in the manner just described be set equal to the geometric downwash along the rear quarter-chord point of the actual wing.

In analytic terms, this requirement results in an integro-differential equation defining the function $\Gamma(y)$. For details, see the discussion in Ref. 4.

e) After the distribution of bound vorticity is calculated, the lift and pitching moment acting at each wing station is determined on the basis of the corresponding expressions from the exact, two-dimensional wing theory. This is in accord with the assumption outlined in (a) above.

Note that if this procedure is followed, the circulatory lift and moment are corrected for aspect ratio effects. However, the apparent-mass terms remain uncorrected, and are those from two-dimensional theory.

2. The earlier discussion outlines the formal aspects of the one-lifting-line theory, and it is now of interest to investigate how the theory

can be organized into a practical calculation scheme. Emphasis is to be placed on the handling of wings of arbitrary planform, including both unswept and swept wings, and wings with either straight or curved quarter- and three-quarter chord lines.

To accomplish this, the approach used by Diederich (Ref. 7) and others, in studying the steady-state loading of thin wings, is extended to the oscillating airfoil case. This consists of essentially replacing the continuous wing vorticity distribution by a series of narrow-span horseshoe vortices, each placed side by side, and each semi-infinite in length in the downstream direction. A schematic representation of the horseshoe vortex pattern is shown in Fig. 2. Note that the mid-span of the leading edge of each horseshoe vortex is situated on the forward quarter-chord line. If the span of each horseshoe is made sufficiently small in comparison with the airfoil span, the errors due to this horseshoe approximation of the continuous vorticity distribution will be small.

The construction of each horseshoe vortex for the oscillating case is considered in detail in Ref. 4. For computational convenience, the span of all the horseshoe vortices are kept equal, and the bound vorticity is kept of constant intensity across the span of each horseshoe.

If the wing is made up of n horseshoe vortices, then the problem of determining the wing loading becomes that of evaluating the n values of bound vorticity for the horseshoes. To accomplish this, n downwash conditions at discrete points can be satisfied. These n points are chosen at the intersection of the rear quarter-chord line of the wing and the n lines defining the mid-span of each horseshoe.

In particular, suppose that the n horseshoe vortices each have a span 2η, and that the $r^{\underline{th}}$ vortex has an intensity of bound vorticity $\Gamma_r e^{i\omega t}$. The positive sense for Γ_r is shown by the arrows in Fig. 2. Now, let Vw_{rs} be the aerodynamic influence coefficient relating the intensity of the $r^{\underline{th}}$ vortex to the downwash at the $s^{\underline{th}}$ downwash satisfaction point. Then, the total downwash at the $s^{\underline{th}}$ point, due to the entire horseshoe pattern for the wing, is

$$w_s^{(t)} = V \sum_{r=1}^{n} w_{rs} \Gamma_r e^{i\omega t} \qquad (2.1)$$

and this must be set equal to the geometric downwash of the wing at point s, i.e.,

can be organized into a practical calculation scheme. Emphasis is to be placed on the handling of wings of arbitrary planform, including both unswept and swept wings, and wings with either straight or curved quarter- and three-quarter chord lines.

To accomplish this, the approach used by Diederich (Ref. 7) and others, in studying the steady-state loading of thin wings, is extended to the oscillating airfoil case. This consists of essentially replacing the continuous wing vorticity distribution by a series of narrow-span horseshoe vortices, each placed side by side, and each semi-infinite in length in the downstream direction. A schematic representation of the horseshoe vortex pattern is shown in Fig. 2. Note that the mid-span of the leading edge of each horseshoe vortex is situated on the forward quarter-chord line. If the span of each horseshoe is made sufficiently small in comparison with the airfoil span, the errors due to this horseshoe approximation of the continuous vorticity distribution will be small.

The construction of each horseshoe vortex for the oscillating case is considered in detail in Ref. 4. For computational convenience, the span of all the horseshoe vortices are kept equal, and the bound vorticity is kept of constant intensity across the span of each horseshoe.

If the wing is made up of n horseshoe vortices, then the problem of determining the wing loading becomes that of evaluating the n values of bound vorticity for the horseshoes. To accomplish this, n downwash conditions at discrete points can be satisfied. These n points are chosen at the intersection of the rear quarter-chord line of the wing and the n lines defining the mid-span of each horseshoe.

In particular, suppose that the n horseshoe vortices each have a span $2j$, and that the $r^{\underline{th}}$ vortex has an intensity of bound vorticity $\Gamma_r e^{i\omega t}$. The positive sense for Γ_r is shown by the arrows in Fig. 2. Now, let Vw_{rs} be the aerodynamic influence coefficient relating the intensity of the $r^{\underline{th}}$ vortex to the downwash at the $s^{\underline{th}}$ downwash satisfaction point. Then, the total downwash at the $s^{\underline{th}}$ point, due to the entire horseshoe pattern for the wing, is

$$w_s(t) = V \sum_{r=1}^{n} w_{rs} \Gamma_r e^{i\omega t} \qquad (2.1)$$

and this must be set equal to the geometric downwash of the wing at point s, i.e.,

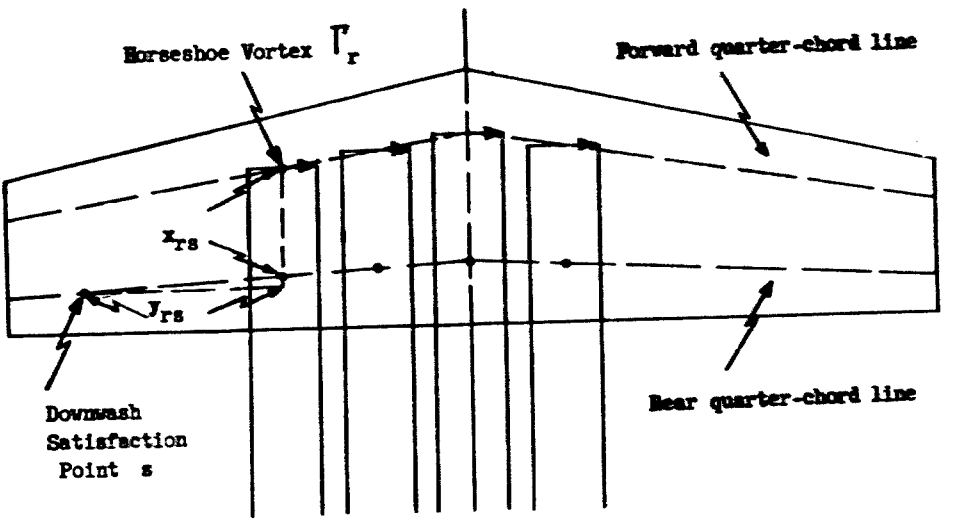

Fig. 2 - Schematic Representation of Replacement of Continuous Vorticity of Single-Lifting-Line Theory by Discrete Horseshoe Vortices.

(The heavy dots are points where the downwash requirements are satisfied.)

$$w_s^{(g)} = \left[\frac{\partial z}{\partial t} + V\frac{\partial z}{\partial x}\right]_s \qquad (2.2)$$

where z is the downward displacement of the wing, and x is a rearward coordinate in the stream direction.

The result of combining Eqs. (2.1) and (2.2) is the m equations in the m unknowns Γ_r,

$$w_s^{(g)} = V\sum_{r=1}^{m} w_{rs}\,\Gamma_r\, e^{i\omega t} \quad , \quad s = 1, 2, \ldots, m \qquad (2.3)$$

In functional terms, it is to be noted that the influence coefficients w_{rs} depend on the variables

$$w_{rs} = z\left[k, \eta, b, x_{rs}, y_{rs}\right] \qquad (2.4)$$

where x_{rs} is the distance the point s lies <u>behind</u> the vortex Γ_r (in the stream direction), and y_{rs} is the distance the point s lies to the <u>right</u> of the mid-span of vortex Γ_r.

The calculation of the w_{rs} is straightforward in theory (see Ref. 4), but entails a considerable amount of computational complexity. As part of the present program, a detailed study has been made of the mathematical character of these aerodynamic influence coefficients, and a convenient means for their accurate tabulatior has been devised. The results of this study are outlined in Appendix II.

Clearly, if the single-lifting-line theory were to be employed in the design office, a complete tabulation of the values of w_{rs} for various k, η/b, x_{rs}/b, y_{rs}/b would be a practical necessity. (It is shown in the Appendix that only a three-parameter tabulation is required.)

3. After the m values of Γ_r have been determined by solution of Eqs. (2.3), the wing lift distribution must be calculated. According to the two-dimensional theory, the <u>circulatory</u> wing lift per unit span, positive in the downward sense, is

$$L = \frac{i}{2}\,\eta' k e^{ik}\left[H_1^{(2)}(k)\right]\rho V \Gamma e^{i\omega t} \qquad (2.5)$$

where $H_1^{(2)}$ is the Hankel function of the second kind and first order. This circulatory lift acts at the local forward quarter-chord line. To get the three-dimensional circulatory lift, the Γ_r values determined from Eq. (2-3) are substituted for Γ in Eq. (2.5). As mentioned earlier, the non-circulatory lift and pitching moment are calculated by two-dimensional strip theory, with no aspect ratio corrections being introduced.

B. Double-Lifting-Line Model

4. As is evident from the prior discussion, the single-lifting-line theory concentrates on the determination of the circulatory wing lift distribution across the airfoil span. However, the theory has two major shortcomings: First, it does not account for movement of the local circulatory center-of-pressure away from the forward quarter-chord line; and secondly, it does not afford aspect-ratio corrections for the apparent mass terms entering into the total wing lift and pitching moment.

At the expense of additional computational complexity, the double-lifting-line theory is an attempt to remedy these shortcomings when calculating aerodynamic wing loadings. The following argument for establishing a two lifting-line wing model has certain aspects in common with the reasoning employed by Holme (Ref. 8) and Multhopp (Ref. 9) for the steady-state case. However, even when applied to a wing in steady-state flow, the present model differs in its details from the Holme discrete-vortex approach. The Multhopp model does not rely on lifting-lines, but on surface vorticity distributions.

5. The wing motion at each spanwise station y (taken in the main stream direction) is assumed to be a combination of pitching motion and plunging motion. Let $B = B(y)$ represent the spanwise variation of the wing pitching amplitude, and let $bA = bA(y)$ be the spanwise variation of the plunging amplitude of the wing at the forward quarter-chord line. Then the instantaneous wing deflection, positive downward, can be written as

$$z = b \cdot e^{i\omega t}\left\{A + (1/2 + \bar{x})B\right\} \qquad (2.6)$$

where ω is the circular frequency of the wing oscillation; t the time coordinate; and $\bar{x}$ is a dimensionless coordinate local to each station, with origin at the mid-chord, and extending chordwise to the rear (i.e., parallel

to the main stream direction). The wing trailing edge is at $\bar{x} = 1$, and the leading edge is at $\bar{x} = -1$.

The downward wing velocity relative to the main stream is then

$$w^{(g)} = \partial z/\partial t + (V/b)\,\partial z/\partial \bar{x} = V \cdot e^{i\omega t}\left\{\bar{P}_o + 2\bar{P}_1 \cos\bar{\theta}\right\} \qquad (2.7)$$

where $\bar{x} = -\cos\bar{\theta}$, V is the main stream velocity, and

$$\bar{P}_o = ikA + \left(1 + \frac{ik}{2}\right) B$$

$$\bar{P}_1 = -\frac{ik}{2} \cdot B$$

where $k = \omega b/V$.

6. The assumption is now made that the wing aerodynamics can be described in terms of "strip" theory, i.e., that each small spanwise segment of the wing behaves as if it were in two-dimensional flow with the chordwise downwash velocity

$$w^{(e)} = w^{(g)} - w^{(i)} \qquad (2.8)$$

Here $w^{(g)}$ is the geometrical downwash velocity of the wing at the station under consideration, and $w^{(i)}$ is the finite-aspect-ratio induction downwash. The "effective" downwash on the wing is then $w^{(e)}$.

It is now further assumed that the finite-aspect-ratio induction downwash can be closely approximated as

$$w^{(i)} = \left[p_o + 2p_1 \cos\bar{\theta}\right] Ve^{i\omega t} \qquad (2.9)$$

where $p_o = p_o(y)$ and $p_1 = p_1(y)$ are functions of the spanwise wing coordinate y. Then the effective downwash becomes

$$w^{(e)} = \left[P_o + 2P_1 \cos \bar{\theta}\right] V e^{i\omega t} \tag{2.10}$$

where $P_o = \bar{P}_o - p_o$ and $P_1 = \bar{P}_1 - p_1$

The results of two-dimensional theory then give, for the chordwise pressure distribution at each station,

$$\Pi = \rho V^2 e^{i\omega t} \left\{ 2a_o \cot \frac{\bar{\theta}}{2} + 4a_1 \sin \bar{\theta} + 2a_2 \sin 2\bar{\theta} \right\} \tag{2.11}$$

where

$$a_o = C(k)(P_o - P_1) + P_1$$

$$a_1 = \frac{1}{2} \; ikP_o - P_1 \; ; \quad a_2 = \frac{1}{2} \; ikP_1$$

and where $C(k)$ is the well known Theodorsen circulation function given by

$$C(k) = \frac{H_1^{(2)}(k)}{H_1^{(2)}(k) + iH_o^{(2)}(k)}$$

The wing lift per unit span, positive downward, is then

$$L = -\rho V^2 e^{i\omega t} \cdot 2\pi b(a_o + a_1)$$

$$= 2\pi \rho V^2 b e^{i\omega t} \left\{ C(k)(P_o - P_1) + \frac{ik}{2} P_o \right\} \tag{2.12}$$

and the nose-up wing moment per unit span about the forward quarter-chord point is

$$M_{c/4} = -\pi\rho V^2 b^2 e^{i\omega t}\left(a_1 - \frac{1}{2}a_2\right)$$

$$= -\pi\rho V^2 b^2 e^{i\omega t}\left\{-P_1 + \frac{ik}{2}\left(P_o - \frac{1}{2}P_1\right)\right\} \tag{2.13}$$

7. It is now of interest to note, from Eq. (2.10) that

$$(P_o - P_1)Ve^{i\omega t} = w^{(e)}_{x=1/2} = w^{(e)}_2 \tag{2.14}$$

where $w^{(e)}_2$ is the effective downwash at the rear quarter-chord point. Also

$$P_o Ve^{i\omega t} = w^{(e)}_{x=0} = w^{(e)}_1 \tag{2.15}$$

where $w^{(e)}_1$ is the effective downwash at the mid-chord point. It also follows that

$$P_1 Ve^{i\omega t} = w^{(e)}_1 - w^{(e)}_2 \tag{2.16}$$

and

$$\left(P_o - \frac{1}{2}P_1\right)Ve^{i\omega t} = \frac{1}{2}\left\{w^{(e)}_2 + w^{(e)}_1\right\} \tag{2.17}$$

The lift and moment per unit span can then be written as

$$L = -2\pi\rho Vb\left\{C(k)w^{(e)}_2 + \frac{ik}{2}w^{(e)}_1\right\} \tag{2.18}$$

$$M_{c/4} = -\pi\rho V b^2\left\{\left(w^{(e)}_2 - w^{(e)}_1\right) + \frac{ik}{4}\left(w^{(e)}_2 + w^{(e)}_1\right)\right\} \tag{2.19}$$

It is thus seen that both the lift and the moment depend only on the values of the effective downwash at the rear quarter-chord point and at the mid-chord point. Note that this conclusion refers to the combination of both circulatory and non-circulatory terms.

6. The construction of the two-lifting-line model can now be examined. It is clear that the chordwise points chosen for downwash satisfaction should be at the mid-chord and rear quarter-chord. The remaining requirements which the construction should satisfy are the following:

(a) For the wing of infinite aspect ratio, the model should give the exact results for lift and moment.

(b) In order that the wake construction for the actual model and the wing be identical, the sum of the circulations of the two lifting lines should equal the wing circulation at each station.

In the interests of setting up a computational procedure of greatest simplicity, the additional restriction will be introduced that the positions of the lifting lines do not change as the reduced frequency k of the oscillation changes.

The best locations for the lifting lines would appear to be those which are exactly correct for the two-dimensional wing in steady-state flow.* If the discrete vortices have the intensities Γ_1 and Γ_2, where

$$\Gamma_1 = \gamma_1 \cdot \cdot V \qquad \text{and} \qquad \Gamma_2 = \gamma_2 \cdot b \cdot V \quad ,$$

and are located at $\bar{x} = \xi_1$ and $\bar{x} = \xi_2$, the equations to be satisfied are

$$\gamma_1 + \gamma_2 = 2\pi \left[w_2^{(g)}/V \right] \tag{2.20}$$

$$\gamma_1/(\xi_1 - 0) + \gamma_2/(\xi_2 - 0) = -2\pi \left[w_1^{(g)}/V \right] \tag{2.21}$$

$$\gamma_1/(\xi_1 - \tfrac{1}{2}) + \gamma_2/(\xi_2 - \tfrac{1}{2}) = -2\pi \left[w_2^{(g)}/V \right] \tag{2.22}$$

These three equations have four unknowns (Γ_1, Γ_2, ξ_1, ξ_2); hence, one unknown may be set arbitrarily. For computational convenience, the location of ξ_2 is set intermediate to the points of downwash satisfaction, i.e., $\xi_2 = 1/4$. It then follows by elimination from Eqs. (2.20) through (2.22) that ξ_1 is determined by

---

* For further discussion of this point, see later discussion.

$$2\xi_1\xi_2\left[1-\frac{w_1^{(g)}}{w_2^{(g)}}\right]-\xi_1-\xi_2=\frac{1}{2} \qquad (2.23)$$

or, since $w_1^{(g)}=w_2^{(g)}$ for steady-state flow about the uncambered profile, and with $\xi_2=1/4$,

$$\xi_1=-\frac{3}{4} \qquad (2.24)$$

i.e., the forward lifting line should be located along the forward one-eighth-chord line.

9. With the locations of the lifting-lines and the points of downwash satisfaction fixed, it is now possible to proceed with the construction of the two-lifting-line model for the oscillating wing. This construction will be accomplished in a fashion analogous to that used earlier for establishing the single-lifting-line model.

Consider first the two-dimensional wing. For a total bound circulation $\Gamma e^{i\omega t}$, the wake construction and wake induction are discussed in Ref. 4. The portion Γ_1/Γ of the wake can be imagined to be associated with the forward lifting line, and the portion Γ_2/Γ can be associated with the rear lifting-line.

As in Ref. 4, for computational convenience, the wake components are to be extended up to the lifting lines themselves. This must be done in such a fashion as to preserve the proper magnitude of the wake vorticity at all points behind the wing trailing edge. At a distance ξ behind the trailing edge, the actual wake vorticity is $ik\Gamma e^{-ik\xi}e^{i\omega t}$.* Now let ξ' and ξ'' be rearward coordinates with origins at Γ_1 and Γ_2, respectively. Extending the wake up to Γ_1 then gives a vorticity distribution of $ik\Gamma_1 e^{-ik(\xi'-7/4)}e^{i\omega t}$ for the Γ_1 wake component; extending the wake up to Γ_2 gives a vorticity distribution of $ik\Gamma_2 e^{-ik(\xi''-3/4)}e^{i\omega t}$ for the Γ_2 wake component.

From Ref. 4, the aerodynamic downwash velocities W_{11} and W_{12} at $\bar{x}=0$ and $\bar{x}=1/2$, respectively, due only to the γ_1 wake are:

Due to γ_1 wake at $\bar{x}=0$,

* See Ref. (5)

$$w_{11/V} = ike^{ik}G(3k/4) \cdot \gamma_1 e^{i\omega t} \cdot \tag{2.25}$$

Due to γ_1 wake at $\bar{x} = 1/2$,

$$w_{12/V} = ike^{ik/2}\, G(5k/4) \cdot \gamma_1 e^{i\omega t} \tag{2.26}$$

Analogously,

Due to γ_2 wake at $\bar{x} = 0$

$$w_{21/V} = ike^{ik}\, G(-k/4) \cdot \gamma_2 e^{i\omega t} \tag{2.27}$$

Due to γ_2 wake at $\bar{x} = 1/2$,

$$w_{22/V} = ik \cdot e^{ik/2} \cdot G(k/4) \cdot \gamma_2 e^{i\omega t} \tag{2.28}$$

where G(u) is defined by (2.37).

Next consider the downwash due to the Γ_1 and Γ_2 lifting lines. In order to construct the model in such fashion that the two-dimensional airfoil theory is exactly duplicated, it will be found necessary to multiply the γ_1 and γ_2 inductions by the semi-empirical factor $\bar{n} = \bar{r}(k)$. Then the downwash contributions w_{11} , etc., of the lifting lines (bound vorticity contributions) at $\bar{x} = 0$ and $\bar{x} = 1/2$ are readily formulated as:

Due to γ_1 at $\bar{x} = 0$: $w_{11/V} = \bar{n}e^{i\omega t}\, \gamma_1 / \{2\pi(3/4)\}$ (2.29)

Due to γ_1 at $\bar{x} = 1/2$: $w_{12/V} = \bar{n}e^{i\omega t}\, \gamma_1 / \{2\pi(5/4)\}$ (2.30)

Due to γ_2 at $\bar{x} = 0$: $w_{21/V} = \bar{n}e^{i\omega t}\, \gamma_2 / \{2\pi(-1/4)\}$ (2.31)

Due to γ_2 at $\bar{x} = 1/2$: $w_{22/V} = \bar{n}e^{i\omega t}\, \gamma_2 / \{2\pi(1/4)\}$ (2.32)

The equations governing the construction of the two-dimensional oscillating wing model are then

$$\gamma_1 + \gamma_2 = (2\pi/\mu) \cdot w_2^{(g)}/V \tag{2.33}$$

$$\gamma_1 \left\{(4/3)\bar{n} + ik \cdot e^{ik} \cdot G(3k/4)\right\} + \gamma_2 \left\{4\bar{n} + ik \cdot e^{ik} \cdot G(-k/4)\right\} = 2\pi \cdot w_1^{(g)}/V \tag{2.34}$$

$$\gamma_1 \left\{(4/5)\bar{n} + ik \cdot e^{\frac{ik}{2}} \cdot G(5k/4) + \gamma_2 \left\{4\bar{n} + ik \cdot e^{\frac{ik}{2}} \cdot G(k/4)\right\} = 2\pi \cdot w_2^{(g)}/V \tag{2.35}$$

where

$$\mu(k) = \frac{1}{2}\pi k \left\{H_0^{(2)}(k) - iH_1^{(2)}(k)\right\} e^{ik} \tag{2.36}$$

and $H_0^{(2)}$, $H_1^{(2)}$ are Hankel functions of the second kind. The function $G(u)$ is defined by the relation

$$G(u) = -\left\{Ci(u) + i\,Si(u) + i\,\pi/2\right\} \tag{2.37}$$

where Si and Ci are the "sinus integralis" and "cosinus integralis" functions, respectively.

Equations (2.33) through (2.35) are three inhomogeneous equations in the three unknowns $\bar{n}$, γ_1, and γ_2. By an evident algebraic manipulation, the three equations can be converted into a quadratic in $\bar{n}$, of the form

$$c_1\bar{n}^2 + c_2\bar{n} + c_3 = 0 \tag{2.38}$$

where the coefficients c_1, c_2 and c_3 are each functions of both k and the ratio $w_1^{(g)}/w_2^{(g)}$. Hence, the $\bar{n}$ roots of the quadratic are likewise dependent on these parameters, i.e.,

$$\bar{n} = \bar{n}\left[k,\ w_1^{(g)}/w_2^{(g)}\right] \tag{2.39}$$

It is now proposed that the factor $\bar{n}$ serve the same role in the two-lifting-line theory that the factor $n(k) \cdot e^{i3k/2}$ serves in the single-lifting-line theory. Thus, the factor $\bar{n}$ is introduced when computing the downwash due to the bound vorticity. When analyzing a wing of infinite aspect-ratio by the two-lifting-line model, the exact results of two-dimensional oscillating wing theory will be duplicated.

Note, however, that $\bar{n}$ depends both on k and on the ratio $w_1^{(s)}/w_2^{(s)}$. The second parameter introduces a quasi-surface type consideration into the two-lifting-line procedure; this, of course, is to be expected from the nature of the construction of the theory.

Note also that the ratio $w_1^{(s)}/w_2^{(s)}$ is determined by the local center of rotation in pitch of each wing station. Hence, for design-office use, a tabulation can be prepared of $\bar{n}$ values for various k and also for various wing rotation centers. Depending on the mode shape, this center of rotation may vary all along the span.

Finally, it is to be noted from Eq. (2.39) that two values of $\bar{n}$ are calculated for each k and $w_1^{(s)}/w_2^{(s)}$ combination. As $k \longrightarrow 0$, one of these values will approach unity, while the other will approach zero. Only the former is a physically admissible $\bar{n}$ value, and this only should be used. Typical values of $\bar{n}$, calculated for pure translatory wing plunging, are shown plotted vs. k in Fig. 3.

10. It is now possible to outline the double-lifting-line procedure for a finite wing of arbitrary planform. The discrete horseshoe vortex is once again used as a basis for the calculation, as a means of simplifying the procedure. Horseshoe vortices are placed along the 1/8- and 5/8-chord lines, as shown schematically in Fig. 4. For convenience, all the horseshoes are made of equal span, and the downwash satisfaction points are taken at the horseshoe midspan stations. The wake for each horseshoe is composed in the same manner as in the preceding Section 9 analysis, and the induction due to each vortex is calculated by adding that due to the wake, plus $\bar{n}$ times the induction due to the concentrated bound vorticity. The manner of computing the downwash at a point on the wing due to each horseshoe vortex is outlined in detail in Appendix II.

Now let m horseshoes be used along the 1/8-chord line, and let m horseshoes be used along the 5/8-chord line. Let their bound vorticity intensities be $\Gamma_{1r}e^{i\omega t}$ and $\Gamma_{2r}e^{i\omega t}$, respectively. Next, define the following aerodynamic influence coefficients:

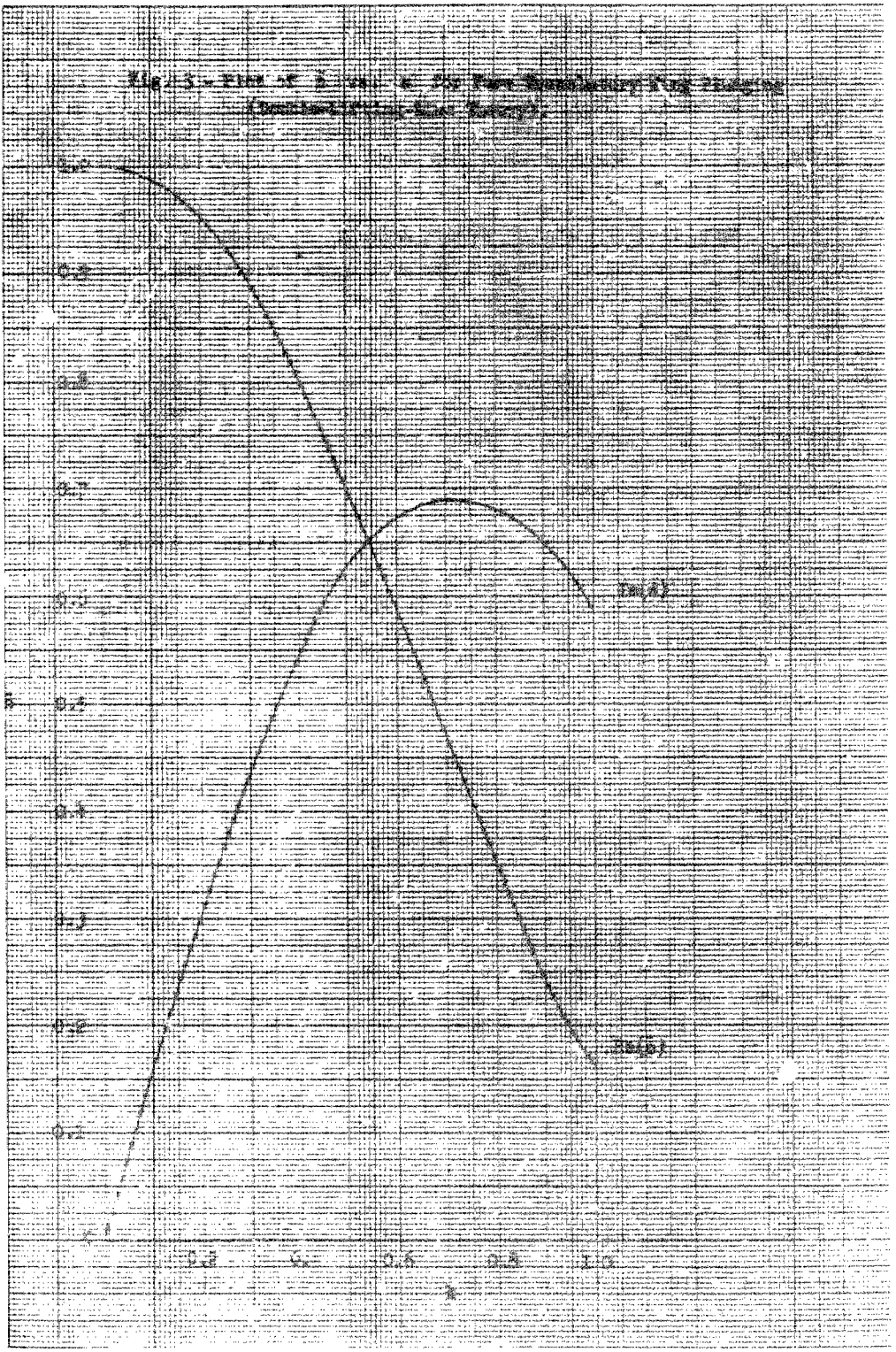

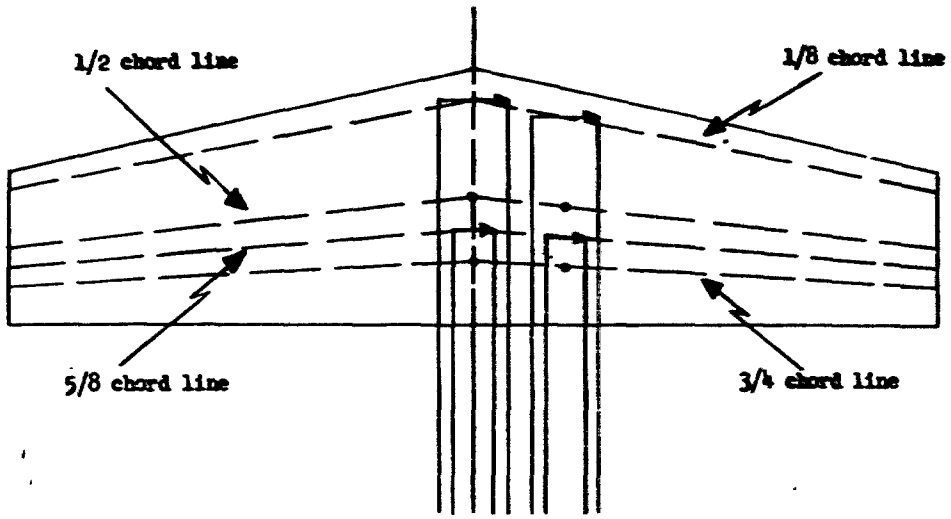

Fig. 4 - Schematic Representation of Horseshoe Vortex System For Double-Lifting-Line Theory.

(The heavy dots are points of downwash satisfaction.)

$Vw_{rs}^{(11)}$ = influence coefficient relating strength of bound vorticity at 1/8-chord at $r^{\underline{th}}$ station to downwash at 1/2-chord at $s^{\underline{th}}$ station.

$Vw_{rs}^{(12)}$ = influence coefficient relating strength of bound vorticity at 1/8-chord at $r^{\underline{th}}$ station to downwash at 3/4-chord at $s^{\underline{th}}$ station.

$Vw_{rs}^{(21)}$ = influence coefficient relating strength of bound vorticity at 5/8-chord at $r^{\underline{th}}$ station to downwash at 1/2-chord at $s^{\underline{th}}$ station.

$Vw_{rs}^{(22)}$ = influence coefficient relating strength of bound vorticity at 5/8-chord at $r^{\underline{th}}$ station to downwash at 3/4-chord at $s^{\underline{th}}$ station.

Then, if $w_{1s}^{(g)}$ is the geometric downwash of the wing at the 1/2-chord line at station s, and $w_{2s}^{(g)}$ is the geometric downwash at the 3/4-chord line at station s, the unknowns Γ_{1r} and Γ_{2r} are determined by the $2m$ equations

$$\left.\begin{aligned} w_{1s}^{(g)} &= V\sum_{r=1}^{m} w_{rs}^{(11)}\,\Gamma_{1r}e^{i\omega t} + V\sum_{r=1}^{m} w_{rs}^{(21)}\,\Gamma_{2r}e^{i\omega t} \\ w_{2s}^{(g)} &= V\sum_{r=1}^{m} w_{rs}^{(12)}\,\Gamma_{1r}e^{i\omega t} + V\sum_{r=1}^{m} w_{rs}^{(22)}\,\Gamma_{2r}e^{i\omega t} \\ & s = 1, 2, \ldots\ldots, m \end{aligned}\right\} \qquad (2.40)$$

The calculation of the influence coefficients $Vw_{rs}^{(11)}$, etc., involves the same complexities as encountered earlier when dealing with the Vw_{rs} of the single-lifting-line theory. Appendix II outlines a procedure for calculating these coefficients on the basis of mathematical functions already tabulated elsewhere, plus certain readily tabulated new functions. For design-office use, a complete tabulation of the Vw_{rs} function would be essential for convenient use of the method.

11. Following calculation of the Γ_{1r} and Γ_{2r} from Eqs. (2.40), it remains to calculate the spanwise distribution of wing lift and pitching moment. This is done through use of Eqs. (2.18) and (2.19).

At a particular station r , the effective downwash velocities $w_2^{(e)}$ and $w_1^{(e)}$ are first calculated. These clearly depend only on the values of Γ_{1r} and Γ_{2r} at that station. From the discussion leading to Eqs. (2.34) and (2.35), it is seen that

$$2\pi \frac{w_{1r}^{(e)}}{V} = \frac{\Gamma_{1r} e^{i\omega t}}{Vb} \left\{ \frac{4}{3} \bar{n} + ike^{ik} G(3k/4) \right\} + \frac{\Gamma_{2r} e^{i\omega t}}{Vb} \left\{ 4\bar{n} + ike^{ik} G(-k/4) \right\} \qquad (2.41)$$

and

$$2\pi \frac{w_{2r}^{(e)}}{V} = \frac{\Gamma_{1r} e^{i\omega t}}{Vb} \left\{ \frac{4}{5} \bar{n} + ike^{ik/2} G(3k/4) \right\} + \frac{\Gamma_{2r} e^{i\omega t}}{Vb} \left\{ 4\bar{n} + ike^{ik/2} G(k/4) \right\} \qquad (2.42)$$

Substitution of $w_{1r}^{(e)}$ and $w_{2r}^{(e)}$ in Eqs. (2.18) and (2.19) yields the local values of L and $M_{c/4}$.

III. FLUTTER ANALYSIS FOR NINE WING MODELS AND A COMPARISON BETWEEN THEORY AND EXPERIMENT

1. In order to appraise the accuracies of the various finite-aspect-ratio aerodynamic theories, flutter analyses were conducted for nine model wings. Each of the model wings were flutter tested in a wind tunnel, so that experimental flutter speeds and frequencies were available for comparison with the calculated values.

The wings dealt with are all of the half-span, "image" type, i.e., the roots of the models were mounted into a plane tunnel wall. The aspect ratios quoted in this report are not for the actual model wing, but are twice as large, representing the model plus its auxiliary "image" half. Hence the aspect ratios correspond to full-span wings fluttering in symmetrical flutter modes.

Of the nine wings, four are of the semi-rigid type, i.e., the airfoil is rigid, and is hinged at its root by means of elastic springs permitting flapping and pitching. Two of these four wings are unswept, while the remaining two have 45° sweep-back, and are derived from the unswept models by simply rotating them by 45°.

The remaining five wings are of the elastic, cantilever type, and were mounted so as to be rigidly built-in at their roots. These wings have sweep-backs ranging between 0° and 45°.

All of the nine wings are of the "uniform wing" variety, i.e., all have unchanging inertial, geometric and elastic properties over their entire span.

A general description of the nine wing models is given in Table II, and a detailed listing of the model parameters if given in Table III. Note that the aspect ratios for the nine wing models range from 2.5 to as high as 8.1.

Note that the ninth wing actually comprises three wind tunnel models, Nos. 9, 9a and 9b. The parameters for wing No. 9 are those of a model scheduled for test at the time these calculations were undertaken. This model was subsequently lost during the tests prior to obtaining any flutter data. Wings Nos. 9a and 9b were to replace No. 9, but their parameters were changed slightly. Also, for the latter wings, a second bending mode unfortunately close to the fundamental torsion frequency made its appearance. (See later discussion)

TABLE II

GENERAL DESCRIPTION OF THE MODEL WINGS

Model	General Description and Reference
1	Model described in USAF Memo Rep. TSEAC5-4595-2-5 (Ref. 10). Unswept uniform wing model with constant chord and of the semi-rigid type. Location of flapping axis: 0.1563 ft inboard from wing root; location of twist axis: 25% of chord, measured from wing leading edge. AR = 8.1.
2	Reference: same as for Model No. 1. Model has 45° sweepback and is of the uniform, semi-rigid type. Model No. 2 is derived from Model No. 1 by rotation of the latter through 45° about the normal to the bending and torsion axes at their point of intersection. Wing tip is normal to the leading edge. AR = 4.1 .
3	Model described in USAF Memo Rep. TSEAC5-4591-5-1 (Ref. 11). Unswept, uniform wing model with constant chord and of the semi-rigid type. Location of flapping axis: 0.3333 ft inboard from wing root; location of twist axis: 35% of chord. AR = 6.2 .
4	Reference: same as for Model No. 3. Model has 45° sweepback and is of the uniform, semi-rigid type, obtained by rotation of Model No. 3 through 45° in the same manner as Model No. 2. Wing tip is normal to the leading edge. AR = 3.1 .
5	Model described in NACA Res. Memo. L50C15a, June 1950, (Ref.18)denoted there as Model 152A. Model is a uniform, unswept wing of the elastic cantilever type. The wing is rigidly built in at the root. AR = 4.0 .
6	Model described in NACA Tech. Note 2121, June 1950, (Ref. 12), denoted there as Model 14A. The model has 45° sweep-back and is of the uniform, elastic cantilever type. Wing is of constant chord and is rigidly built in at the root. Wing tip is parallel to the main flow. AR = 4.0 .

TABLE II (Concluded)

Model	General Description and Reference
7	Model described in NACA Tech. Note 2121 (Ref. 12) denoted there as Model 13. Wing is of the uniform elastic cantilever type, has 30° sweep-back, and has a wing tip parallel to the stream direction. AR = 4.0 .
8	Model described in NACA Tech. Note 2121 (Ref. 12), denoted there as Model 22'B. Model is of the uniform, elastic cantilever type, has 15° sweep-back, and has its wing tip parallel to the stream direction. AR = 4.0 .
9	Model described in Supplemental Agreement S 2(53-321) under the present contract, denoted there as Example No. 3. Wing is of the uniform, elastic cantilever type, with streamwise tip, and 45° sweep-back. AR = 2.5 .
9a, 9b	Models similar to above No. 9, and described as Models III and IV, respectively, in WADC letter, WCLSY, 1 July 1953, present contract.

TABLE III

NUMERICAL PARAMETERS FOR THE NINE MODEL WINGS

(Units are: Force in lb.; length in ft.; time in sec.; angles in rad; mass in slugs.)

	Model 1	Model 2	Model 3	Model 4	Model 5	Model 6	Model 7	Model 8	Model 9	Model 9a	Model 9b
AR	8.113	4.056	6.222	3.111	4.0	4.0	4.0	4.0	2.5	2.5	2.5
b	0.370	0.523	0.375	0.530	0.333	0.333	0.333	0.333	0.236	0.236	0.236
s	3.0	2.121	2.333	1.650	1.333	1.333	1.333	1.333	0.590	0.590	0.590
γ^o	0	45	0	45	0	45	30	15	45	45	45
d	0	0	0.2	0.2	0.126	0.42	0.42	0.348	0.294	0.294	0.294
m	0.0316	0.0316	0.0759	0.0810	0.0155	0.0096	0.01352	0.00603	0.00851	0.00851	0.00851
S	0.0048	0.0048	0.00376	0.00401	0.00185	0.000126	0.000215	0.00025	0.00117	0.00102	0.00133
I	0.00108	0.00108	0.00477	0.00430	0.000654	0.000121	0.000251	0.00018	0.0000185	0.0000185	0.0000185
ω_p	20.94	20.94	34.03	26.81	181.0	138.23	207.3	194.8	49.6	38.6*	40.0*
ω_q	69.33	69.33	110.46	92.93	321.1	578.05	584.3	389.6	240.0	204.2*	216.4*
$g^{(p)}$	0.02	0.02	0.01	0.01	0.0258	0.02	0.02	0.02	0.02	0.015	0.015
$g^{(q)}$	0.02	0.02	0.01	0.01	0.0221	0.03	0.03	0.03	0.02	0.015	0.015
M	0	0	0.36	0.36	0.254	0.56	0.62	0.34	0	0.19	0.20
ρ	0.002374	0.002374	0.00115	0.00115	0.00215	0.00720	0.00746	0.00488	0.00150	0.00210	0.00216
V_{exp}	88.0	110.0	395.8	407.7	292.6	287.3	295.0	174.0	--	211.0	220.3
ω_{exp}	49.2	60.2	73.64	64.53	281.5	339.3	383.0	320.0	--	138.2	136.1

TABLE III (Concluded)

Let CG and EA denote distances wing center of gravity and elastic axis respectively lie aft of leading edge, each given as a percentage of the wing chord. Let r_{α} be radius of gyration of wing about elastic axis as a percentage of the wing semi-chord. Designate by μ, the ratio of the mass of the wing to the mass of a cylinder of air circumscribed about the wing chord, both extending over equal span lengths. Then the parameters d, m, S and I employed above may be replaced by an equivalent set as follows:

	Model 1	Model 2	Model 3	Model 4	Model 5	Model 6	Model 7	Model 8	Model 9	Model 9a	Model 9b
μ	31.0	31.0	149	160	20.6	7.8	7.2	3.8	65	66.7	65.5
EA	25	25	35	35	31.3	46.0	46.0	42.4	39.7	40.6	38.8
CG	45	45	41.6	41.6	49.2	48.8	48.8	48.8	46.6	47.5	46.8
r_{α}^2	0.484	0.484	0.456	0.419	0.380	0.23	0.23	0.292	0.28	0.274	0.275

* These are measured coupled frequencies. The third coupled frequencies for models 9a and 9b are 230.4 and 244.3 rads/sec, respectively. The mode is essentially second bending.

2. All of the flutter analyses were conducted on a two degree-of-freedom basis, employing the fundamental, uncoupled wing bending and fundamental, uncoupled wing torsion modes as the generalized coordinates. Since the wings had been chosen so that the frequencies of all higher modes are well above the frequencies of these fundamental modes, the use of a two degree-of-freedom analysis is justifiable. (As already mentioned, this condition was violated through error in Models 9a and 9b. See later discussion.)

The mode shapes for the elastic cantilever models were not determined experimentally, but were instead arrived at by theoretical calculation. The wings being uniform, the shapes in question merely correspond to the fundamental bending mode and the fundamental torsion mode for a uniform bar.

Estimates of the damping coefficients appropriate for the various modes were supplied by the sponsoring agency, after inspection of the models, or were determined by actual decay tests.

Since all of the flutter analyses are based on incompressible air forces, a correction for compressibility effects is required before comparison can be made between the calculated and experimental results. This was done on the basis of the Prandtl-Glauert rule, in the manner outlined in Ref. 2.

3. In the interest of brevity, the detailed calculations for the various analyses are not presented here. However, the following remarks outline the manner in which they were carried out.

The equations of motion were derived in conventional fashion, in the manner outlined by Smilg and Wasserman (Ref. 2) for the unswept wing, and by Spielberg, Pettis and Toney (Ref. 13) and Pettis (Ref. 3) for the swept wing. The aerodynamic treatments in these references are all based on two-dimensional strip theory; when a different aerodynamic theory is employed, the generalized forces in Refs. 2, 3 and 13 must be reinterpreted accordingly. The necessary theoretical changes are evident and need not be dealt with in detail here.

In the work which follows, when reference is made to the "two-dimensional strip method", it is implied that the aerodynamic treatment is based on two-dimensional strip theory, the strips being taken in the streamwise direction. The calculational procedures are described in detail in Refs. 2, 3 and 13.

The natures of the "Wasserman-Reissner" and "Wasserman-Biot" aerodynamic treatments are outlined in Appendix I. The two differ only in that the former uses the Reissner theory (Refs. 5 and 6) to determine $(F + \frac{1}{3}G)_3$,

while the latter makes use of the Biot-Boehnlein theory (Ref. 14) for this determination. The manner in which these aerodynamic approaches are introduced into the flutter analysis is discussed in Appendix I. In both cases the steady three-dimensional circulation distributions were calculated by the Weissinger method using 15 points across the span.

Considering next the "single-lifting-line method", this is obviously based aerodynamically on the theory given in the preceding section of this report. For the numerics, the wing span (which equals twice the actual span of the half-image models) was divided into eleven equal increments. A discrete, oscillating horseshoe vortex was employed within each of these eleven spanwise intervals, and the downwash satisfaction points were chosen at the mid-span of each interval. This affords eleven points of downwash satisfaction, equal in number to the number of vortices employed. Note that the central downwash point then falls at the exact mid-span of the wing. The downwash influence coefficients for the single-lifting-line method were calculated in the manner described in Appendix II.

In carrying out the aerodynamic analyses, advantage was taken of the symmetrical character of the flutter modes. By symmetry considerations it is evident that the intensities of each pair of "image" vortices are equal; hence, only the intensities of six of the eleven horseshoe vortices require evaluation by solution of simultaneous equations.

Once the spanwise distributions of lift and pitching-moment were evaluated for each of the generalized coordinates, the technique of flutter analysis was carried out in the Ref. 2 manner.

Finally, for the double-lifting-line calculations, eleven discrete horseshoe vortices of equal span were distributed along the one-eighth chord line, and eleven equal-span vortices were distributed along the five-eighths chord line. The downwash influence coefficients were calculated according to the Appendix II formulae.

In evaluating the bound vorticity intensities, symmetry considerations permitted the number of simultaneous equations requiring solution to be reduced from twenty-two to twelve. Nonetheless, it is evident that calculations by the two-lifting-line approach are tedious and require that automatic calculation techniques be enlisted for convenience.

4. A summary of the results of the flutter analyses for the nine wings is given in Tables IV to VIII. The first two tables list the calculated and experimental flutter speeds and frequencies, while Table VI and VII give the ratios of the calculated and observed values. Table VIII lists the computed and experimental reduced speeds $V/b\omega$.

TABLE IV

VALUES OF CALCULATED AND EXPERIMENTAL FLUTTER SPEEDS

(Units of velocity are ft /sec)

Method / Model	Two-Dimensional Strip $V_{th}^{(c)}$	Wasserman-Reissner $V_{th}^{(c)}$	Wasserman-Biot $V_{th}^{(c)}$	Single-Lifting-Line $V_{th}^{(c)}$	Double-Lifting-Line $V_{th}^{(c)}$	Experimental Flutter Speed V_{exp}
1	84.0	95.9	100.0	--	--	88.0
2	97.9	128.3	141.9	--	--	110.0
3	366.4	419.7	437.4	--	--	395.8
4	269.9	390.1	433.7	--	--	407.7
5	259.3	341.7	355.2	336.5	318.0	297.0
6	194.7	235.6	280.1	288.4	--	287.3
7	188.0	--	--	288.0	--	295.0
8	140.0	--	--	199.0	--	174.0
9	168.5	--	--	194.7	--	--
9a	--	--	--	--	--	211.0
9b	154.0* 146.7**	--	--	175.6***	--	220.3

* Two degree of freedom analysis using measured coupled modes. (See p. 25)

** Three degree of freedom analysis using uncoupled first and second bending and first torsion mode shapes of a uniform beam.

*** Extrapolated from Model 9 results assuming $V/B\omega_\alpha$ at flutter remains constant for both models. Note that if this technique is applied to the two-dimensional strip values, then for Model 9b, $V = (168.5)(216.4)(240.0) = 151.8$ ft./sec.

TABLE V

VALUES OF CALCULATED AND EXPERIMENTAL FLUTTER FREQUENCIES

(Units of frequency are rads/sec)

Model \ Method	Two-Dimensional Strip	Wasserman-Reissner	Wasserman-Biot	Single-Lifting Line	Double-Lifting Line	Experimental Flutter Frequency
	ω_{th}	ω_{th}	ω_{th}	ω_{th}	ω_{th}	ω_{exp}
1	40.9	44.0	46.6	--	--	49.2
2	48.7	48.1	47.6	--	--	60.2
3	64.2	71.1	69.2	--	--	73.6
4	55.3	65.4	67.3	--	--	64.5
5	273.1	267.7	301.3	275.9	221.0	281.5
6	419.8	391.2	375.2	337.6	--	339.3
7	407.0	--	--	320.0	--	383.0
8	311.0	--	--	290.0	--	320.0
9	168.7	--	--	122.0	--	
9a	--	--	--	--	--	138.2
9b	144.5* 135.7**	--	--	--	--	136.1

*, ** See p. 29

TABLE VI

RATIOS OF CALCULATED AND EXPERIMENTAL VALUES OF THE FLUTTER SPEEDS

Model \ Method	Two-Dimensional Strip	Wasserman-Reissner	Wasserman-Biot	Single-Lifting Line	Double-Lifting Line	Experimental Flutter Speed
	$V^{(c)}_{th}/V_{exp}$	$V^{(c)}_{th}/V_{exp}$	$V^{(c)}_{th}/_{exp}$	$V^{(c)}_{th}/_{exp}$	$V^{(c)}_{th}//V_{exp}$	V_{exp} (ft/sec)
1	0.96	1.09	1.14	--	--	88.0
2	0.89	1.17	1.29	--	--	110.0
3	0.93	1.06	1.11	--	--	395.8
4	0.66	0.96	1.07	--	--	407.7
5	0.89	1.17	1.21	1.150	1.07	297.0
6	0.68	0.82	0.98	1.004	--	287.3
7	0.64	--	--	0.970	--	295.0
8	0.80	--	--	1.140	--	174.0
9	--	--	--	--	--	--
9a	--	--	--	--	--	211.0
9b	0.70* 0.67**	--	--	--	--	220.3

*, ** See p. 29

TABLE VII

RATIOS OF CALCULATED AND EXPERIMENTAL VALUES OF THE FLUTTER FREQUENCIES

Method / Model	Two-Dimensional Strip	Wasserman-Reissner	Wasserman-Biot	Single-Lifting Line	Double-Lifting Line	Experimental Flutter Frequency
	ω_{th}/ω_{exp}	ω_{th}/ω_{exp}	ω_{th}/ω_{exp}	ω_{th}/ω_{exp}	ω_{th}/ω_{exp}	ω_{exp} (rads/sec)
1	0.83	0.89	0.95	--	--	49.2
2	0.81	0.80	0.79	--	--	60.2
3	0.87	0.97	0.94	--	--	73.6
4	0.86	1.01	1.04	--	--	64,5
5	0.97	0.95	1.07	0.980	0.79	281.5
6	1.24	1.15	1.11	0.995	--	339.3
7	1.06	--	--	0.840	--	383.0
8	0.97	--	--	0.910	--	320.0
9	--	--	--	--	--	--
9a	--	--	--	--	--	138.2
9b	1.06* 1.00**	--	--	--	--	136.1

*, ** See p.29

TABLE VIII

VALUES OF CALCULATED AND EXPERIMENTAL REDUCED SPEEDS $V/b\omega$

(b is measured perpendicular to leading edge)

Method / Model	Two-Dimensional Strip $(V/b\omega)_{th}$	Wasserman-Reissner $(V/b\omega)_{th}$	Wasserman-Biot $(V/b\omega)_{th}$	Single-Lifting Line $(V/b\omega)_{th}$	Double-Lifting Line $(V/b\omega)_{th}$	Experimental Reduced Speed $(V/b\omega)_{exp}$
1	5.55	5.89	5.80	--	--	4.83
2	5.43	7.21	8.06	--	--	4.94
3	15.23	15.76	16.88	--	--	14.34
4	13.03	15.91	17.28	--	--	16.96
5	2.85	3.83	3.54	3.65	4.32	3.16
6	1.97	2.55	3.17	3.62	--	3.59
7	1.60	--	--	3.12	--	2.67
8	1.40	--	--	2.13	--	1.69
9	5.99	--	--	9.56	--	--
9a	--	--	--	--	--	9.16
9b	6.39* 6.49**	--	--	--	--	9.71

*, ** See p. 29

A typical V-g diagram, for wing Model 5, is shown in Fig. 5. The mode shapes for this wing are given in Fig. 6, while Figs. 7-12 present some results of the aerodynamic calculations for Model 5 according to both the single-and-double-lifting line theories.

These Model 5 results are fairly typical of the various wing calculations, and Figs. 5-13 are intended to give some physical insight into the character of the aerodynamic performance of the wing according to the single-and-double-lifting line theories.

An analysis of the conclusions indicated by Tables IV to VIII and Figs. 5-12 is left for the next section of the report.

5. A word of explanation is in order as to why each wing was not flutter-analyzed on the basis of all the aerodynamic theories employed in the study. The program was started with the aim of evaluating the merits of the Wasserman procedures by flutter-analyzing Models 1-6 by two-dimensional strip theory, and by the Wasserman-Biot and Wasserman-Reissner procedures. While these calculations were under way, the single-lifting-line approach was developed.

The single-lifting-line theory was not applied to Models 1-4, since question had arisen regarding the nature of the flow in the root region of these semi-rigid wing models, and the accuracy of conventional, image-type flutter analyses was open to argument. Hence, Models 5 and 6 were studied by the new theory, Models 7-9 being added after the preliminary trials showed promise.

Finally, when the double-lifting-line theory was developed, only Model 5 was analyzed prior to conclusion of the program. This model was chosen, since it was felt that the initial exploration of the theory should be based on an unswept wing.

III. DISCUSSION

1. In evaluating the merits of the various methods for flutter analysis, the appraisal should be made from two standpoints: First, from the designer's point of view, which method gives closest correlation with the experimental flutter speeds? This, obviously, is the criterion of most pressing interest to the practicing engineer. Of secondary importance, mainly as further evidence of the dependability of a promising method and for use in such instances as the planning of flight-flutter tests, interest is also centered in whether the flutter speed correlation is accompanied by agreement between the calculated and observed flutter frequencies and mode shapes.

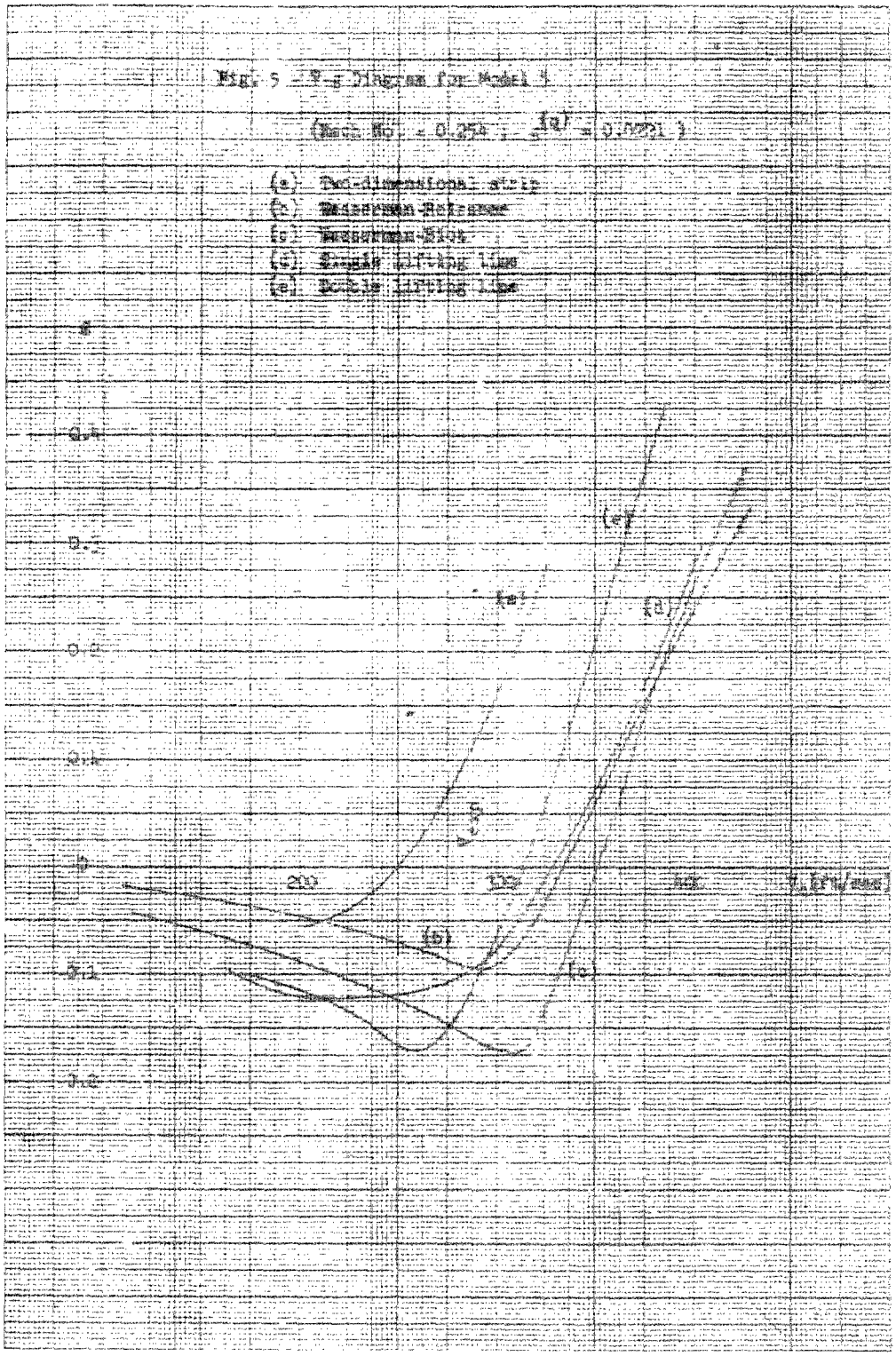
(a) Two-dimensional strip
(b) Prandtl-Reissner
(c) Prandtl-Mises
(d) Single slip-line line
(e) Double slip-line line
(a)
(b)
(c)
(d)
(e)
200
300
400

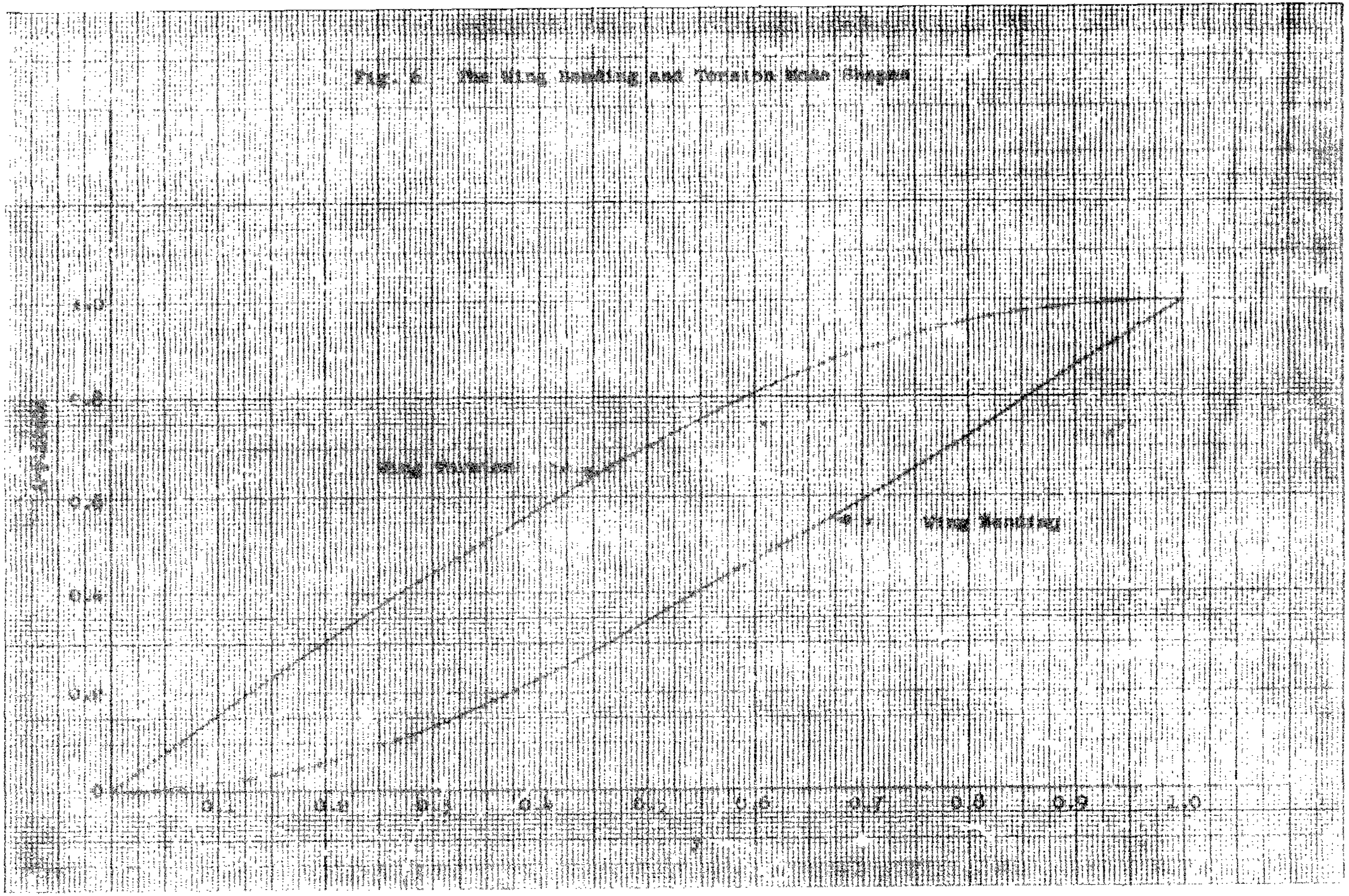

Fig. 6 The Wing Bending and Torsion Mode Shapes

Fig. 7 - Spanwise distributions of dimensionless wing circulation for the Model 1 bending mode, as calculated by the single- and double-lifting-line theories. The latter is shown by a solid line k=0.25.

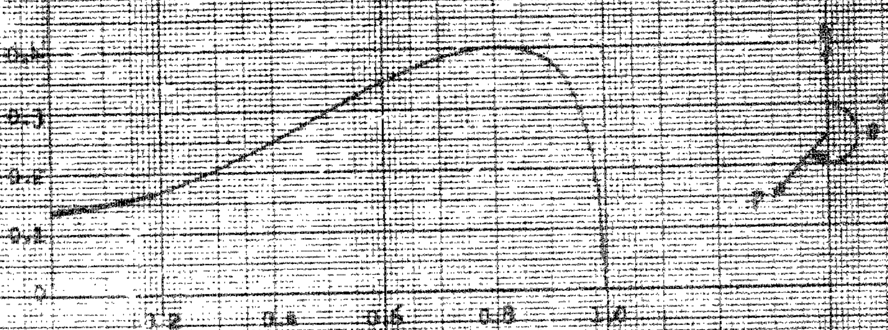

(a) Amplitude Distribution

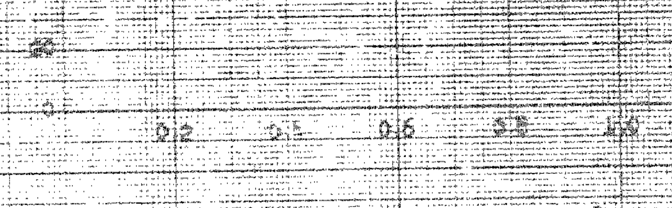

(b) Phase Distribution, β°

Fig. 8 - Spanwise distributions of dimensionless w.g. circulation for the Mode 5 torsion mode, as calculated by the single and double-lifting-line theories. The latter is shown by a solid line. x=0.25

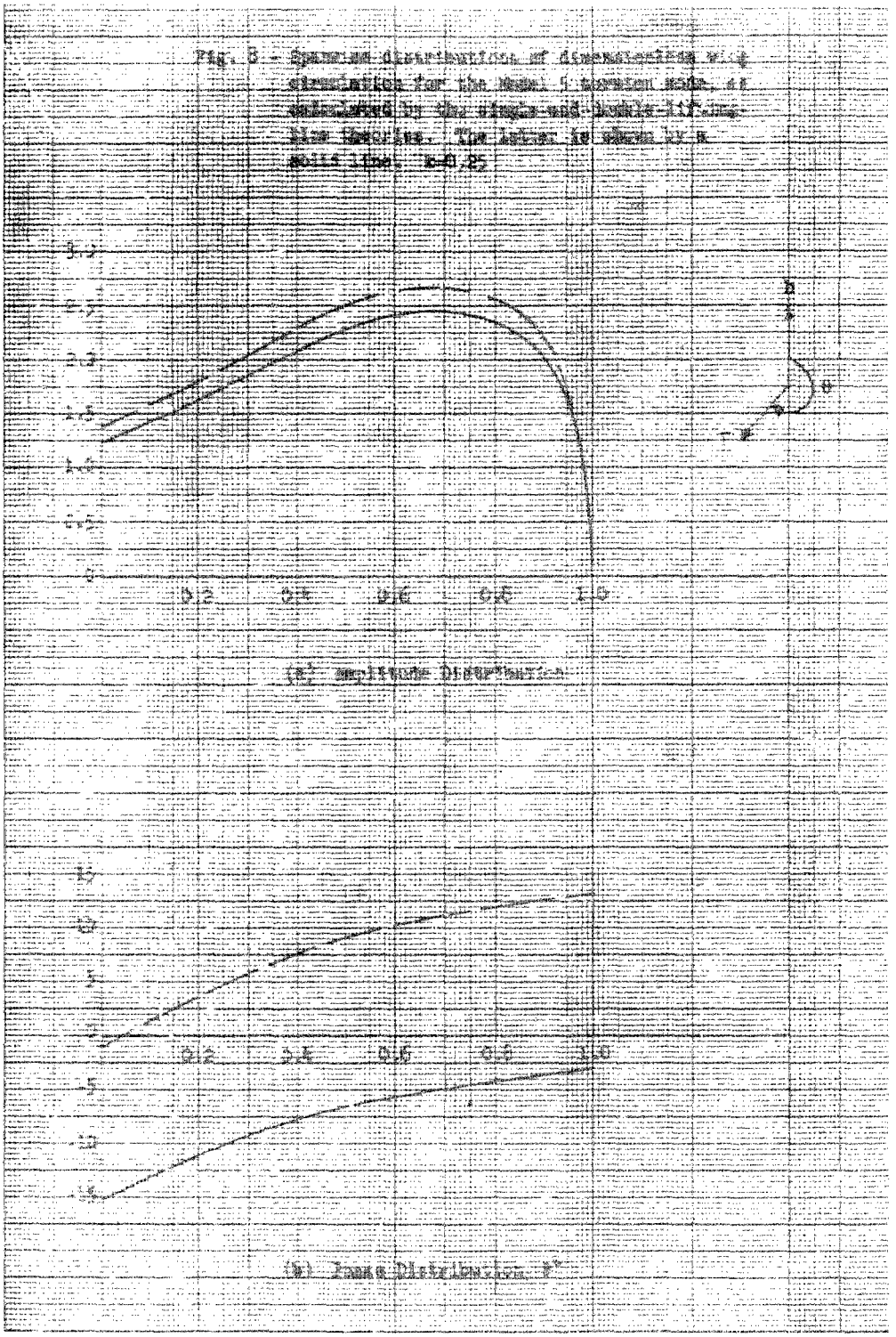

(a) Amplitude Distribution

(b) Phase Distribution, ϕ°

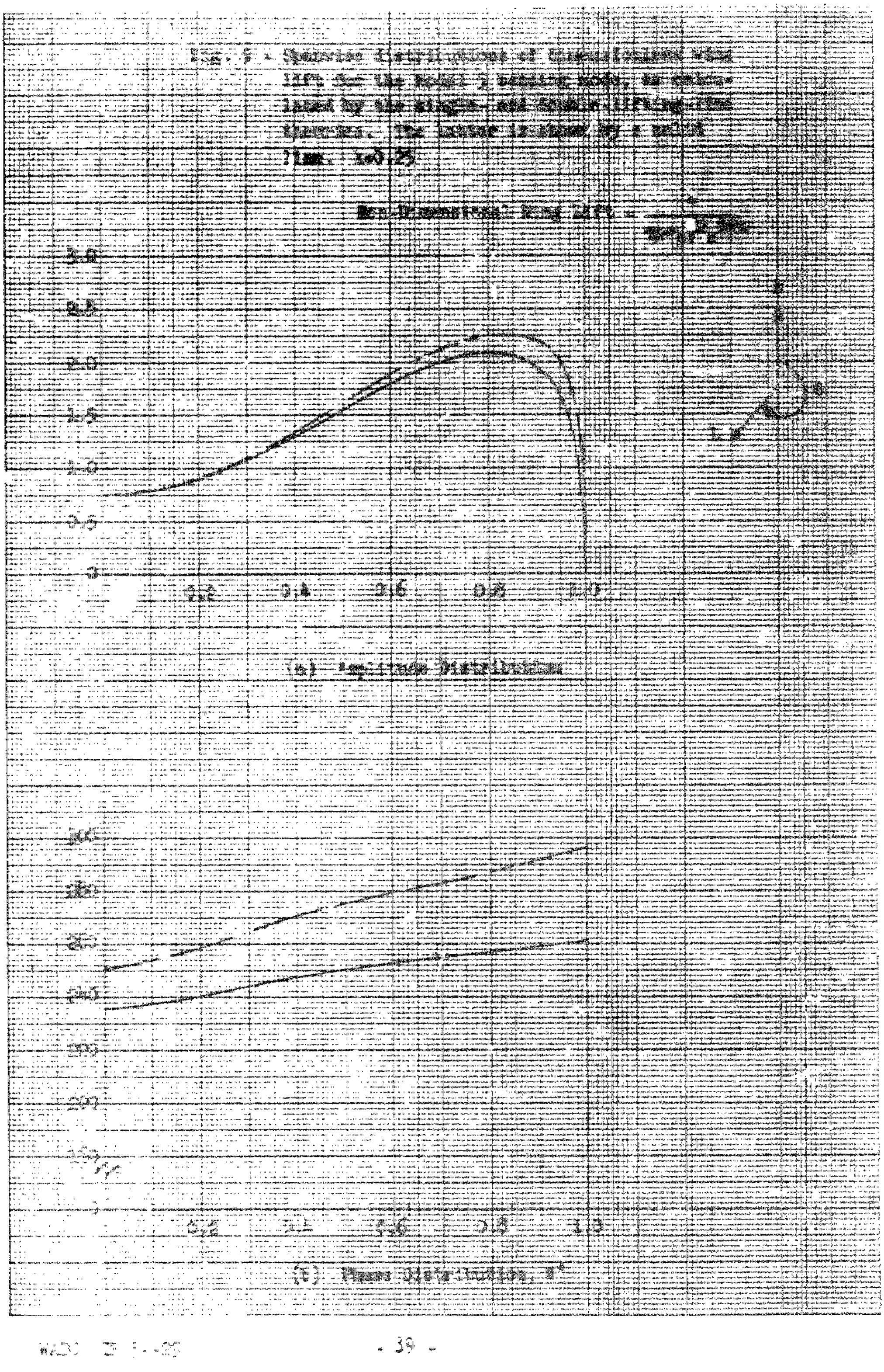

Fig. 5 - Spanwise Distributions of [illegible] Wing Lift for the Model 1 bending mode, as calculated by the single- and double-lifting-line theories. The latter is shown by a solid line. k=0.25

Fig. 30 - Spanwise distributions of dimensionless wing lift for the model 5 horizontal pods, as related by the single- and double-triangular theories. The latter is shown by a solid line, $k=0.35$.

Nondimensional Wing Lift = $\frac{L}{\rho V^2 c_r^2}$

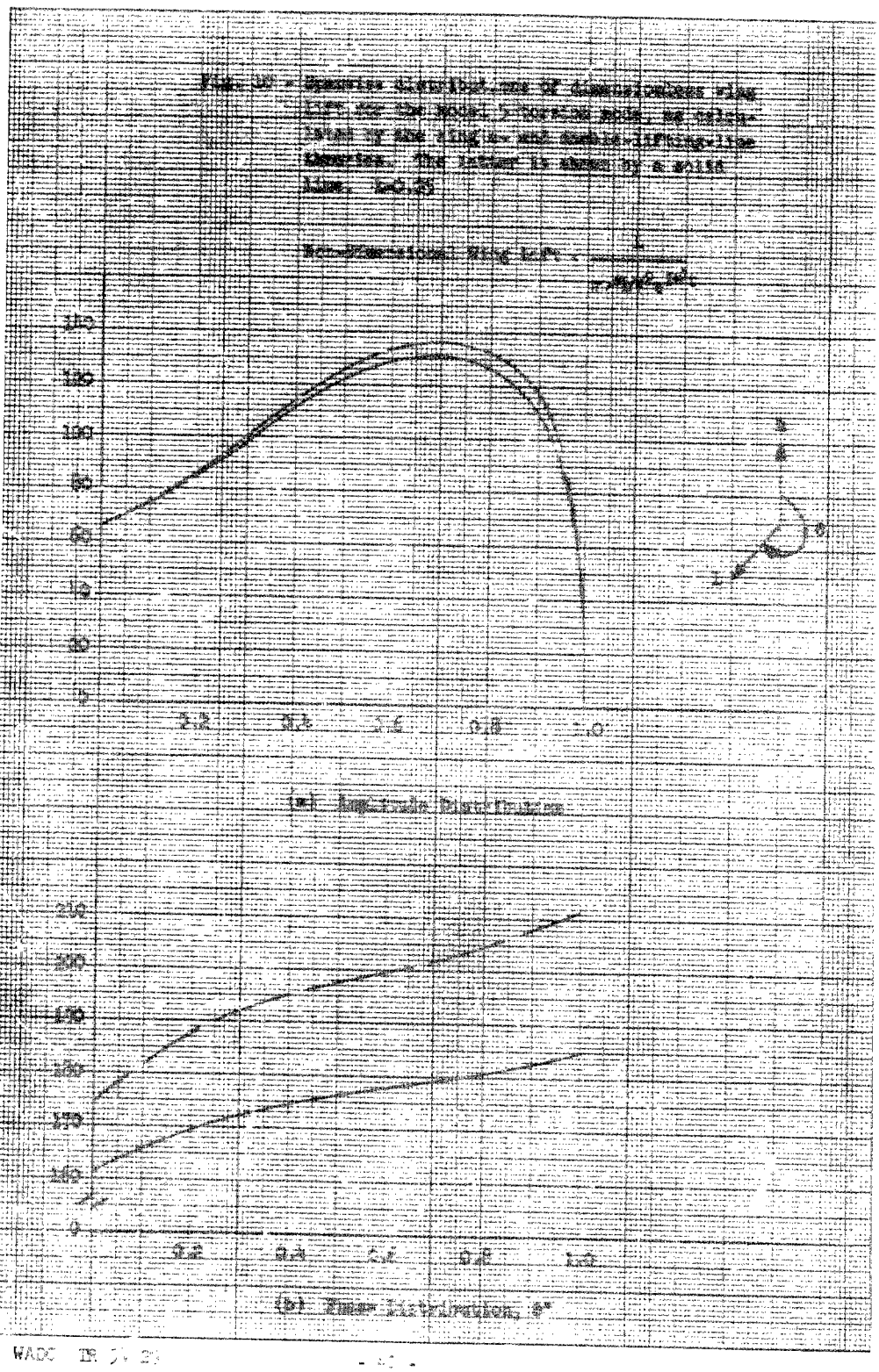

Fig. 2 - Spanwise distributions of aerodynamic wing moment about the quarter-chord line for the model 5 bending mode, as calculated by the single- and double-lifting-line theories. The latter is shown by a solid line. $M=2.25$

$$\text{Non-dimensional wing moment} = \frac{M_{c/4}}{\rho_\infty V_\infty^2 b^2 \Delta z}$$

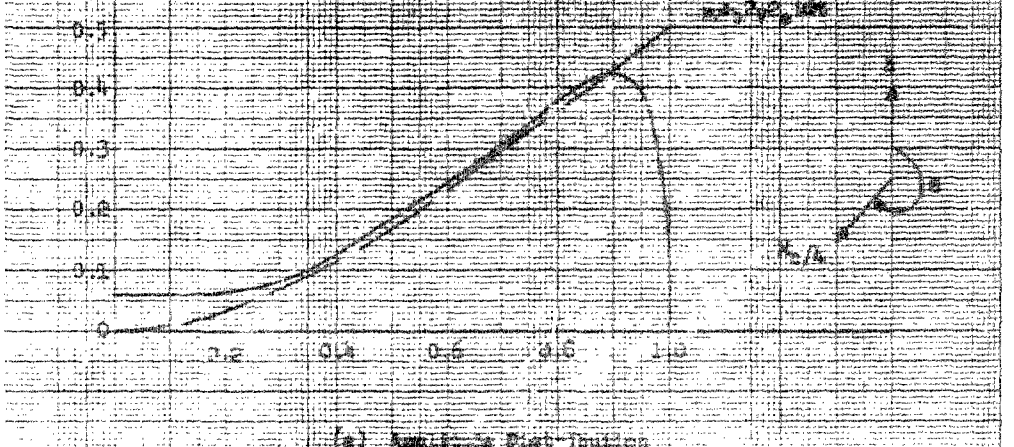

(a) Aerodynamic Wing-Torque

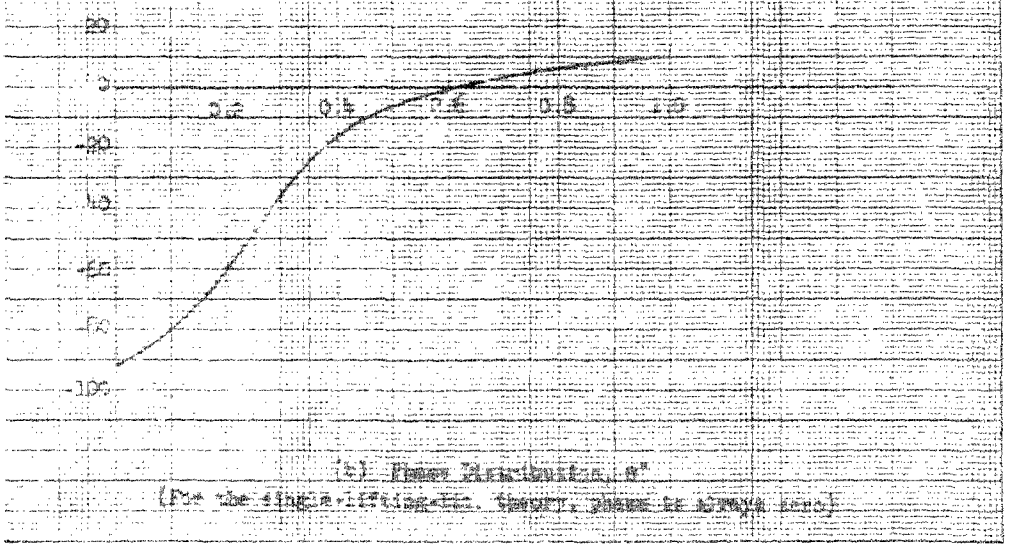

(b) Phase Distribution, φ

(For the single-lifting-line theory, phase is always zero)

Fig. 12 - Spanwise distributions of discontinuous wing moment about the quarter-chord line for the Model 3 vibration mode, as calculated by the kinetic- and Kussner-lifting-line theories. The latter is shown by a solid line. $k=0.25$.

Non-dimensional Wing Moment $= \dfrac{M_{c/4}}{\pi \rho_\infty c^2 \omega^2 a_0 w_0}$

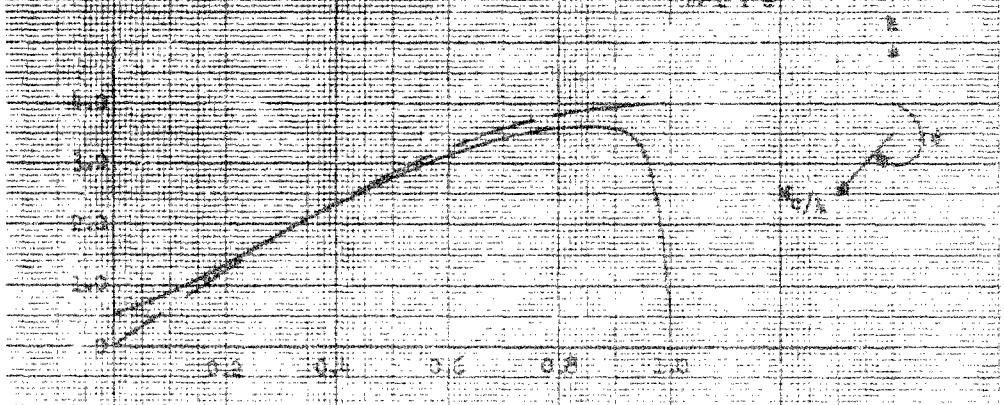

(a) Amplitude Distribution

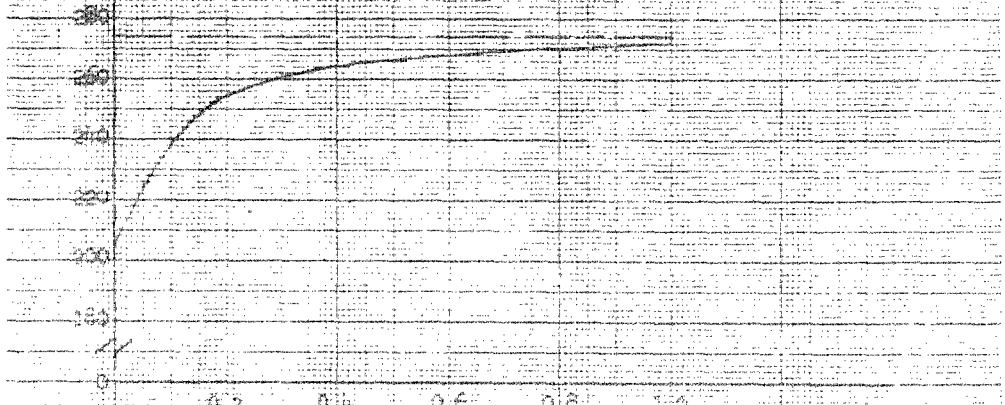

(b) Phase Distribution, θ°

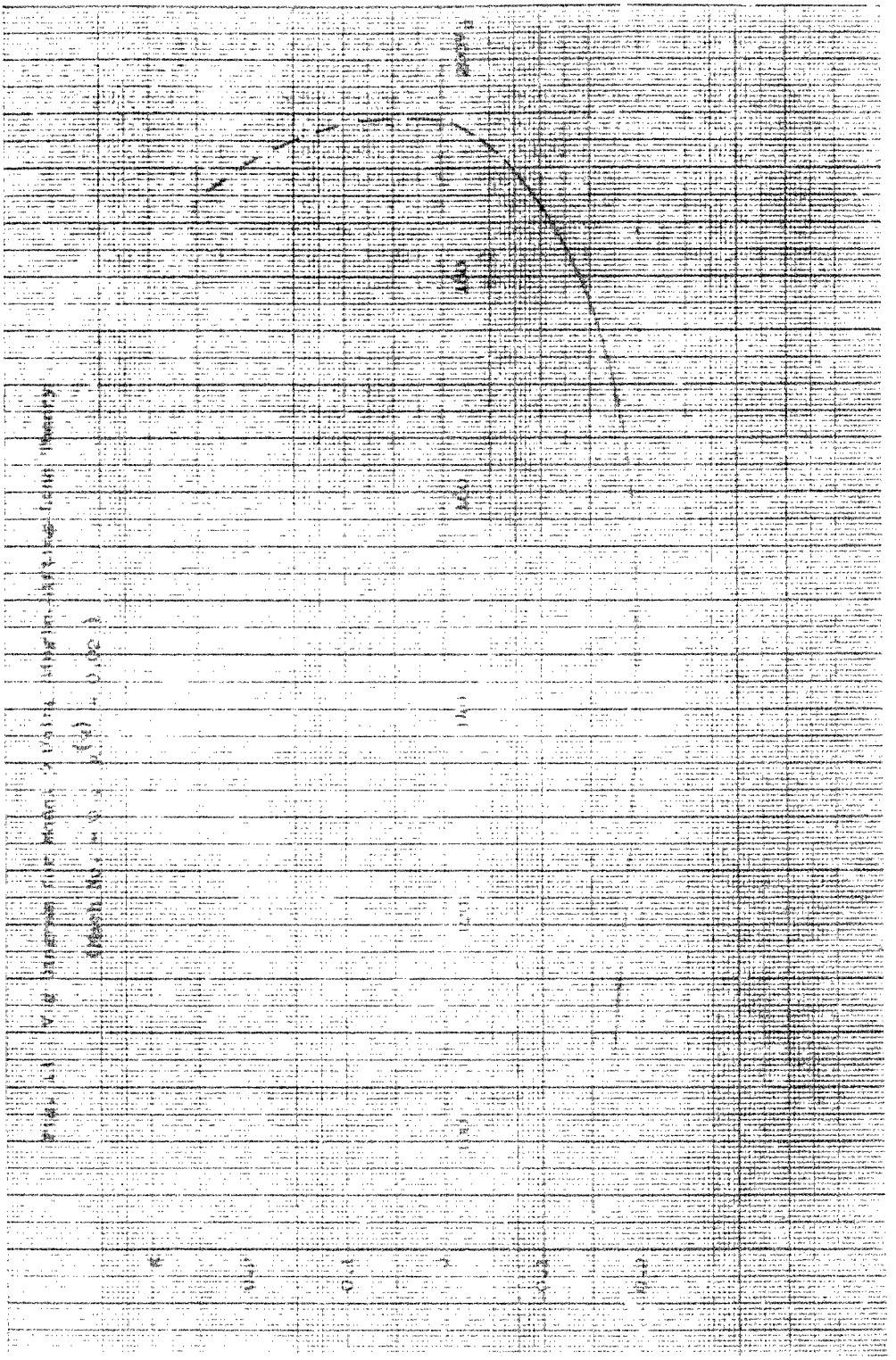

A second basis for evaluation is from a more research-minded standpoint and centers around the choice of a method which best described the details of the physical phenomena involved in the flutter mechanism. In the present studies, it is felt that the inertial and elastic portions of the mechanism are described with good accuracy; hence, the character of the results should be indicative of the success achieved by the various methods in describing the aerodynamic phases of the problem. In general, it is to be expected that the quality of the flutter predictions will improve as the aerodynamic treatment becomes more nearly theoretically valid, and it is interesting to analyze the present findings to determine whether they confirm this expectation.

2. Before proceeding with the evaluation of the worth of the various flutter analysis methods, it should be recognized that conclusions are to be based on a comparison of calculated and experimental flutter data; hence, the accuracy of the latter is of cardinal importance. In particular, the merit of a calculated value of flutter speed or frequency must be appraised by comparison with the observed value plus or minus the applicable range of uncertainty of the experimental measurements.

In the case of the models dealt with here, there is every reason to believe that the various test agencies used both care and skill in constructing the test items and in carrying out the flutter tests. Hence, the accuracies of the observations are undoubtedly representative of the very finest of current test practice.

3. It is now pertinent to examine the results shown in Tables IV through VIII. As a starting point, consider the unswept wing models, i.e., Models 1, 3 and 5.

Models 1 and 3 were analyzed only by the two-dimensional strip method and by the two variations of the Wasserman procedure; Model 5, on the other hand, was analyzed on the basis of all of the aerodynamic theories treated in this study.

Consider first the results obtained from two-dimensional strip theory. For the unswept wings, the predicted flutter speeds are always conservative, i.e., are always lower than the observed values. This, of course, is a desirable feature for a design procedure, providing the degree of conservatism is not large. For Models 1 and 3, the extent of conservatism is on the order of 5 per cent, while the flutter speed prediction for Model 5 appears to be about 10 per cent low.

The flutter frequency predictions by strip theory for Models 1 and 3 appear to be definitely low, by some 10 - 15%, while a surprisingly close

frequency prediction is achieved for Model 5.

Turning next to the two Wasserman procedures, it is seen that the flutter speed predictions are all unconservative, i.e., too high. It will become apparent in the later discussion that this is an undesirable characteristic of virtually all the flutter predictions based on the finite aspect-ratio aerodynamic treatments. Comparing the two Wasserman-type methods, it is clear that the Wasserman-Reissner variant is superior to the Wasserman-Biot. For Model 3, the Wasserman-Reissner flutter speed prediction is about 5% high (unconservative), while the Model 1 and 5 predictions appear to be some 10 - 15% high.

As regards flutter frequency, the Wasserman procedures appear to result in better agreement with the observed values than does the two-dimensional strip method. On the other hand, most of the predictions lie outside the range of experimental uncertainty.

The Model 5 calculation based on the single-lifting theory appears to offer a slight improvement over the Wasserman-Reissner calculation, both with regard to flutter speed and frequency, although the speed prediction continues to be undesirably unconservative. It is pointed out in Ref. 4 that the principle advantages of this theory should arise in the treatment of sharply swept wings, and this will be borne out in the later discussion.

Because of the tedious nature of the associated numerics, only one wing was analyzed on the basis of the two-lifting-line theory, this being Model 5. The results show a definite improvement in flutter speed prediction over all the other finite-aspect-ratio calculations, the flutter speed being in error by about 5%, although on the unconservative side.

On the other hand, the flutter frequency predicted by the two-lifting-line procedure is some 15% low. This result is a disappointing one, and is discussed in more detail later in this section.

As a general conclusion the preceding results tend to indicate that design office flutter analyses of unswept wings should employ two-dimensional strip theory in preference to any of the finite span flutter theories tried here. This method is a well known one, is relatively simple to apply, and also affords results of good accuracy and moderate conservatism. It is interesting to note that this conclusion merely confirms general practice, which is based on the broad experience of many design-office analysts.

4. Having examined the unswept cases, it is next of interest to inspect the results for the most highly swept wings, i.e., Models 2, 4, 6 and 9, all with 45° sweepback.

An examination of the flutter predictions for Models 2, 4, 6 and 9b shows at once that the use of two-dimensional strip theory for sharply swept wings is generally unsatisfactory. With regard to flutter speed, the results for Model 2 are satisfactory, but the predictions for Models 4, 6, and 9b are conservative to the unacceptable extent of some 35%. The flutter frequency predictions by this method are also poor.

Considering next the Wasserman-Reissner results, it is seen that flutter speed predictions on this basis for the 45° swept wings fall in the range of from 80 - 120% of the experimental values. For Models 2, 4, 6, the recorded flutter speed errors are 18%, -4% and -18%, respectively. The flutter frequency errors for the same models are -20%, +1%, and +15%, respectively. The excellent predictions of both flutter speed and frequency for Model 4 would appear to be coincidental; in general, application of the Wasserman-Reissner technique to sharply swept wings does not seem promising (see later discussion).

The second Wasserman variant, namely, the Wasserman-Biot method, also does not appear to give results which agree with the experimental observations with any consistency.

Turning now to the single-lifting-line theory, calculations are available for Models 6 and 9. For Model 6, both the speed and frequency are predicted with excellent accuracy. For Model 9, the agreement between calculations and the Models 9a and 9b experiments is not good, but this may not be due to incorrectness on the part of the aerodynamic theory. As already noted, the second bending modes for Models 9a and 9b have frequencies close to the first torsion mode. Hence, for accuracy, a three degree-of-freedom analysis may be required, whereas the present results are for only a two degree-of-freedom treatment.

In order to check the validity of two degree-of-freedom calculations for Model 9b, personnel of the Dynamics Branch, Aircraft Laboratory, WADC, conducted two-dimensional, strip theory calculations taking into account (a) only the fundamental bending and torsion modes, and (b) the first two bending modes plus the fundamental torsion mode. The results of these calculations are shown in Tables IV-VIII, and tend to indicate that neglect of the second bending mode as a degree-of-freedom does not lead to serious error. Hence, the opinion expressed in the preceding paragraph may be unduly pessimistic.

5. An examination of Models 7 and 8 is now of interest. Model 7 has 30° sweepback. Using two-dimensional strip theory, the calculated flutter speed is approximately 35% conservative. This is in general accord with the results obtained for the 45° swept wings. On the other hand, the single-lifting-line theory yields quite excellent flutter speed prediction, although disappointing flutter frequency estimation.

Model 8 has 15° sweepback. By two-dimensional strip theory, a 20% conservative flutter speed is predicted, while the flutter frequency prediction is accurate within the range of experimental uncertainty. The single-lifting-line theory gives results which are 1% unconservative in flutter speed, and which are 9% in error in flutter frequency.

6. It is thus seen from the swept wing studies that a convincing argument emerges against the use of two-dimensional strip theory for sharply swept wings. Also, both Wasserman procedures appear to lead to erratic predictions which are generally unsatisfactory.

The single-lifting-line theory appears to offer most promise for sharply swept wings, as is indicated by the results for Models 6 and 7. However, even with this theory, the flutter frequency predictions are not consistently satisfactory.

7. Finally, consider the various aerodynamic treatments from the point of view of their theoretical merit. The Wasserman procedures are clearly semi-empirical, as is evident from the Appendix I discussion. Hence, they are difficult to appraise on purely rational grounds.

As regards the two-dimensional strip method, this is characterized by neglect of the aerodynamic inter-action between the vorticity patterns at and behind the various wing stations, i.e., each wing station "sees" a two-dimensional (infinite span) vorticity distribution. It is to be expected that this approach will lead to the greatest error for sharply swept wings (see Ref. 4), and the present results confirm this in convincing fashion. On the other hand, for unswept wings of moderate to large aspect-ratio, the errors will be smaller, and in fact appear to be within the range of the required design office accuracy.

The single-lifting-line theory was developed to have particular applicability to sharply swept wings. For such cases, it has a generally rational foundation. On this basis, the satisfactory agreement in predicted flutter speeds by this method for Models 6 and 7 is not surprising. However, the poor agreement in flutter frequency for Model 7 is surprising.

The double-lifting-line theory should be the most theoretically satisfactory of all the methods dealt with in this program. However, the Model 5 results do not appear to bear out this expectation, and because of the elaborate nature of the calculations required for the method, only this single case could be attempted.

An oddity of the Model 5 calculation by the double-lifting-line theory is worthy of special mention. As is well known, the characteristic roots of the stability (flutter) determinant for a two-degree-of-freedom analysis are two in number. In the method of flutter analysis employed in this study, the reduced speed $V/b\omega$ is used as a variable parameter in determining the values of the determinant elements. A plot of the characteristic roots vs. $V/b\omega$ thus yields two distinct stability "branches", and one of these branches leads to the flutter condition.

It was noted that the double-lifting-line calculations lead to flutter along a different branch than do the calculations by all the other methods. This resulted in "doubling back" of the $V/b\omega$ vs. g plot, which is an unusual behavior for a wing bending-torsion flutter case. The reasons for this could not be resolved, although special effort was made to insure that the double-lifting-line computations are free from error.

8. An examination of Figs. 7-12 is now of interest as a means of comparing the predicted aerodynamic performance of an unswept wing on the basis of the single-and-double-lifting-line theories.

Figs. 7 and 8 show that the magnitudes of the spanwise distribution of wing circulation for the bending and torsion modes, according to the two theories, do not differ greatly. This is to be generally expected. On the other hand, particularly for the torsion mode, marked phase differences between the two circulation distributions are encountered.

The spanwise life distributions for the two modes as shown in Figs. 9 and 10, show substantial differences when calculated by the two methods. Note that the two-lifting-line method leads to greater tip-unloading than does the one-lifting-line procedure.

Finally, Figs. 11 and 12 show the spanwise moment distributions for the two modes, as calculated from the two theories. The differences between the two methods are quite evident here, in line with the theoretical expectation. It is interesting to note, however, how the agreement in calculated moments improves as the wing tip region is approached.

IV. CONCLUSIONS: RECOMMENDATIONS FOR FURTHER RESEARCH

1. On the basis of the studies reported here, the following conclusions appear in order:

a) For unswept, or slightly swept wings with moderate to large aspect ratio, design office subsonic flutter calculations should presently be based on two-dimensional strip theory for the aerodynamic treatment. A moderate and acceptable degree of conservatism is to be expected in the flutter speeds predicted on this basis. The predicted flutter frequencies will not, however, be dependable.

b) The Wasserman procedure, the single-lifting-line method, and the double-lifting-line method should not be used for the flutter analysis of unswept or slightly swept wings of reasonable to large aspect ratio.

c) For sharply swept wings (say 25° or greater sweep) with moderate to large aspect ratio, the single-lifting-line theory presently offers most promise for the aerodynamic treatment of the subsonic flutter problem. However, this conclusion must be regarded as tentative until further confirmation is achieved by additional trials. In general, the calculated flutter speeds will be considerably more dependable than the calculated flutter frequencies.

d) The Wasserman procedures appear to be unacceptable for the treatment of wings with substantial sweep.

2. The following recommendations are made regarding further desirable research studies:

a) The single-lifting-line theory should be applied to additional swept wing cases, in order to further evaluate its accuracy and dependability.

Should the theory continue to show good accuracy in flutter speed prediction, the method should be routinized for design office use.

b) The various aspects of the double-lifting-line theory should be further examined, and calculations for swept wings should be carried out.

c) When dependable measurements become available of the spanwise distribution of lift and pitching moment on oscillating wings, these results should be compared with the predictions of the single- and double-lifting-line theories. Such comparisons will permit direct evaluation of these theories, and may also point out the directions to be taken toward improved aerodynamic treatments.

REFERENCES

1. Wasserman, L. S., "Aspect Ratio Corrections in Flutter Calculations", AMC Memo. Report No. MCREXA5-4595-8-5, August, 1948.

2. Smilg, B., and Wasserman, L. S., "Application of Three-Dimensional Flutter Theory to Aircraft Structures", AAF Tech. Report 4798, July, 1942.

3. Pettis, H. E., "The Effect of Sweepback on the Critical Flutter Speed of Wings", AMC Memo. Report No. TSEAC5-4595-2-9, May, 1946.

4. Dengler, M. A., and Goland, M., "The Subsonic Calculation of Circulatory Spanwise Loadings for Oscillating Airfoils by Lifting-Line Techniques", Journal of the Aeronautical Sciences, Vol. 19, No. 11, pp. 751-759, November, 1952.

5. Reissner, E., "Effect of Finite Span on the Airload Distribution for Oscillating Wings. I - Aerodynamic Theory of Oscillating Wings of Finite Span", NACA Tech. Note No. 1194, March, 1947.

6. Reissner, E., and Stevens, J. E., "Effect of Finite Span on the Airload Distribution for Oscillating Wings, II - Methods of Calculation and Examples of Application", NACA Tech. Note No. 1195, October, 1947.

7. Diederich, F. W., "Charts and Tables for Use in Calculations of Downwash of Wings of Arbitrary Plan Form", NACA Tech. Note No. 2353, May, 1951.

8. Holme, Olaf A. M., "On the Approximate Solution of the Lifting Surface Problem With the Aid of Discrete Vortices", Division of Aeronautics, Royal Inst. Tech., Stockholm 26, March 29, 1949, KTH-Aero TN 6.

9. Multhopp, H., "Methods for Calculating the Lift Distribution of Wings" (Subsonic Lifting Surface Theory), Royal Aircraft Establishment, Farnsborough, January, 1950. RAE Report No. Aero 2353

10. Kramer, E. E., "The Effect of Sweepback on the Critical Flutter Speed of Wings", AMC Memo. Report No. TSEAC5-4595-2-5, March, 1946.

11. Tolve, L. A., "Transonic Flutter Model Tests", AMC Memo. Report No. TSEAC5-4591-5-1, August, 1947.

12. Barmby, J. B., Cunningham, H. J., and Garrick, I. E., "Study of Effects of Sweep on the Flutter of Cantilever Wings", NACA Tech. Note No. 2121, June, 1950. Also available as NACA TR 1014, 1951.

REFERENCES (Concluded)

13. Spielberg, I., Pettis, H. E., and Toney, H. S., "Methods for Calculating the Flutter and Vibration Characteristics of Swept Wings", AMC Memo. Report No. MCREXA5-4595-8-4, August, 1948.

14. Biot, M. A., and Boehnlein, "Aerodynamic Theory of the Oscillating Wing of Finite Span", GALCIT Report No. 5, September, 1942.

15. Luke, Y. L., and Ufford, D., "A Table of the Complete Cicala Function", Journal of the Aeronautical Sciences, Vol. 20, July, 1953, pp. 511 - 512.

16. Dengler, M. A., Goland, M., and Luke, Y. L., "Tables of the Functions $\int_0^y (e^{iu} - 1) \sqrt{u^2 + b^2}\, du/u$ ", Midwest Research Institute Report, August, 1952.

17. Harvard Computation Laboratory, "Tables of the Complete Cicala Function", Problem Report No. 58 (AF Problem 77), October, 1952.

18. Widnayer, E., Jr., Lanten, W. T., Jr., and Clevenson, S. A., "Experimental Investigation of the Effect of Aspect Ratio and Mach Number on the Flutter of Cantilever Wings", NACA RM L50C15a, 1 June 1950.

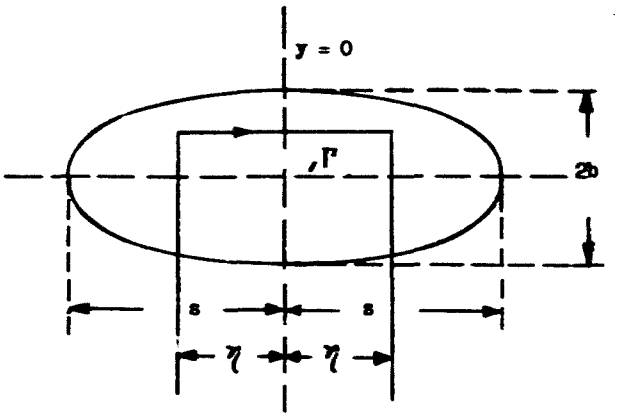

$$\rho V\Gamma = \frac{1}{2}\rho V \cdot 2b \cdot V\alpha C_{L_{2D}} = \frac{1}{2}\rho V \cdot 2b \cdot 2\pi(V\alpha - w_i) \qquad (I.2)$$

$$w_i = w_{i\Gamma} = \frac{\Gamma}{2\pi\eta} \qquad (I.3)$$

where $C_{L_{2D}}$ is the <u>local</u> lift-coefficient-slope of the wing, Γ is the intensity of the horseshoe vortex, w_i is the induced downwash on the wing at the root, $w_{i\Gamma}$ is the induced downwash at the root arising from Γ, and ρ, V have the obvious definitions.

Now, in line with Eq. (I.1), assume that

$$\frac{C_{L_{2D}}}{2\pi} = \frac{AR}{AR + 2} \qquad (I.4)$$

Eqs. (I-2)-(I.4) can be considered as three equations in the three unknowns η', Γ, C_{L_α}, and their solution leads to the result

$$\frac{\eta}{b} = \frac{AR}{2} \qquad (4.5)$$

Wasserman now assumes that the original wing is rectangular, so that $AR = S/b$, and hence

$$\frac{\gamma}{S} = \frac{1}{2} \tag{I.6}$$

Note that if the original wing were taken as elliptic, then Eq. (I.5) would lead to

$$\frac{\gamma}{S} = \frac{1}{2\pi} \tag{I.7}$$

It is of further interest to note that if the condition of the same lift per unit span is replaced by the condition of the same total lift from the wing and horseshoe vortex, then it can be shown that, for all wings,

$$\frac{\gamma}{S} = \frac{1}{\sqrt{2}} \tag{I.8}$$

Wasserman, however, constructs his system on the basis of Eq. (I.6), presuming a rectangular wing.

d) Step 4 - Recourse is now made to some of the results derived in other treatments of the same problem. For example, the work of Reissner (Refs. 5, 6), which follows a more rigorous line of reasoning, may be employed. In the present study, the work of Reissner and of Biot and Boehmlein (Ref. 14) is utilized for the step to be described here.

Considering a rectangular wing, with circulation distribution corresponding to the horseshoe vortex of uniform intensity constructed in Step 3, either the Reissner or the Biot and Boehmlein theory is used to derive an $(F + iG)_3$ which represents the behavior of the three-dimensional wing. For each wing aspect-ratio and for each reduced frequency, an appropriate $(F + iG)_3$ value can be computed without difficulty. For a detailed discussion of how this is accomplished, see Wasserman's original treatment, Ref. 1.

Tables of $(F + iG)_3$ vs. AR vs. reduced frequency can now be prepared for easy reference, so that for any values of "effective aspect ratio" and reduced frequency, the appropriate $(F + iG)_3$ can be directly read off.

e) Step 5 - Returning now to the ΔR distribution determined along the wing span in Step 2, and for each reduced frequency of interest, the spanwise distribution of $(F + iG)_3$ is now determined by means of the tables of Step 4.

The $(F + iG)_3$ distribution so obtained is then used in place of the Theodorsen C(k) function in the equations for the two-dimensional air forces. The air forces computed on this basis are used in the flutter analysis.

f) Step 6 - It is evident that the preceding method for deriving $(F + iG)_3$, and hence the air forces, is straightforward when the ratio $\gamma/\bar{\gamma}$ is less than one. However, it is also possible to obtain values of the $\gamma/\bar{\gamma}$ ratio which are greater than one. Equation (I.4) then leads to negative ΔR values, which are obviously not admissible.

Under this circumstance, Wasserman suggests that the ratio $\gamma/\bar{\gamma}$ be taken as the true ratio of circulation for the oscillatory case.

Another difficulty in the method arises when $\bar{\gamma}$ is zero. In this event, calculate $\gamma/\bar{\gamma}_r$, where $\bar{\gamma}_r$ is the two-dimensional circulation at a chosen reference station. Then, $(\gamma/b)/(\bar{\gamma}_r/b_r)$ is taken as the ratio of the induced downwash to the circulatory downwash at the reference station, b being the local semi-chord in each case.

It is to be noted that a separate air force determination is required for each wing mode of interest and for each reduced frequency. However, once the steady-state circulation distributions are calculated, the remainder of the process becomes simple and direct, and does not involve any laborious solutions of sets of simultaneous equations, as in the case of the more rigorous methods of calculation. From the point of view of design-office practice, the Wasserman procedure is an acceptable one. However, unless it can be conclusively demonstrated that very superior accuracy can be achieved through their use, the more rigorous methods must be classed as impractical because of the considerable labor they entail.

APPENDIX II

CALCULATION OF THE AERODYNAMIC INFLUENCE COEFFICIENTS w_{rs} FOR THE ONE- AND TWO-LIFTING LINE THEORIES

1. By using the techniques described in Ref. 4, it can be shown that the downwash induced by a rectangular, oscillating, horseshoe vortex with bound circulation $\bar{\Gamma} e^{i\omega t}$ and span 2η is given by

$$\bar{w} e^{i\omega t} = \left[\bar{w}_b + \bar{w}_w\right] e^{i\omega t} \tag{II.1}$$

where $\bar{w}_b$ describes the induction due to the concentrated bound vortex filament, and $\bar{w}_w$ describes the downwash arising from the wake trailing behind the bound vortex.

Using the coordinate system shown in Fig. 14, the value of $\bar{w}_b$ at a point (x, y) can be shown to equal

$$\bar{w}_b = \frac{\bar{\Gamma}}{4\pi x}\left[\frac{\eta + y}{R_1(x)} + \frac{\eta - y}{R_2(x)}\right] \tag{II.2}$$

where

$$R_1(x) = \left[x^2 + (\eta + y)^2\right]^{1/2}$$

$$R_2(x) = \left[x^2 + (\eta - y)^2\right]^{1/2}$$

The value of $\bar{w}_w$ is found to be, for $|y| < \eta$,

$$\bar{w}_w = \frac{\bar{\Gamma}}{4\pi}\left[\frac{2\eta}{\eta^2 - y^2} e^{-ikx} + \frac{x}{(\eta+y)R_1(x)} + \frac{x}{(\eta-y)R_2(x)}\right.$$

$$-ike^{-ikx}\left[F[k(\eta + y)] + F[k(\eta - y)] + E[k(\eta + y)]\right.$$

$$\left.\left. + E[k(\eta - y)]\right\}\right] \tag{II.3}$$

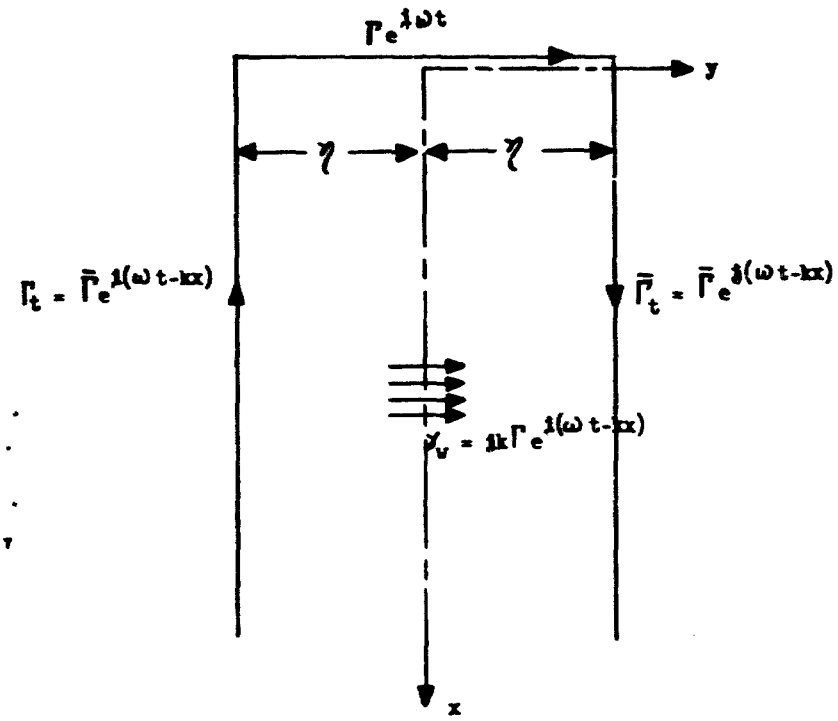

Fig. 14 - Schematic Diagram of Vorticity Associated With a Rectangular, Oscillating, Horseshoe Vortex.

while for $|y| > \eta$,

$$\bar{v}_k = \frac{\bar{\Gamma}}{4\pi}\left[\frac{2\eta}{\eta^2 - y^2}e^{-ikx} + \frac{x}{(\eta + y)R_1(x)} + \frac{x}{(\eta - y)R_2(x)}\right.$$

$$- ike^{-ikx}\left\{P\left[k(y+\eta)\right] - P\left[k(y-\eta)\right] + H\left[k(y+\eta)\right]\right.$$

$$\left.\left. - H\left[k(y-\eta)\right]\right\}\right] \qquad (II.4)$$

where $P[k\zeta]$ is the complete Cicala function

$$P(k\zeta) = \int_0^\infty e^{-i\lambda}\left\{\frac{1}{k\zeta} + \frac{1}{\lambda} - \frac{\sqrt{\lambda^2 + (k\zeta)^2}}{\lambda(k\zeta)}\right\} d\lambda \qquad (II.5)$$

and $H[k\zeta]$ is a related incomplete function

$$H(k\zeta) = \int_{-\infty}^0 e^{-i\lambda}\left\{\frac{1}{\lambda} - \frac{\sqrt{\lambda^2 + (k\zeta)^2}}{\lambda(k\zeta)}\right\} d\lambda \qquad (II.6)$$

2. The manner of arriving at the aerodynamic influence coefficients $\bar{w}_{rs}$, for the single and double lifting line theories is now evident from the discussion given in the body of the report, and from the expressions Eqs. (II.1)-(II.4).

After much manipulation, the coefficient $\bar{w}_{rs}$ can be cast into the following form which is convenient for calculation:

<u>One-Lifting-Line Theory</u>

$$\bar{w}_{rs} = \frac{\bar{\Gamma}}{4\pi\eta}\left\{\frac{1}{v+1}\left[\frac{s(k)}{\varepsilon_1\sqrt{1+\varepsilon_1^2}} + \frac{\varepsilon_1}{\sqrt{1+\varepsilon_1^2}} + e^{-ib_1\varepsilon_1}\left\{1 - \frac{ib_1}{2}\log\left(\frac{\varepsilon_1}{1+\sqrt{1+\varepsilon_1^2}}\right)^2\right\}\right.\right.$$

$$\left.- iD(\varepsilon_1, b_1)\right] - \frac{1}{v-1}\left[\frac{s(k)}{\varepsilon_2\sqrt{1+\varepsilon_2^2}} + \frac{\varepsilon_2}{\sqrt{1+\varepsilon_2^2}} + e^{-ib_2\varepsilon_2}\left\{1 - \frac{ib_2}{2}\log\left(\frac{\varepsilon_2}{1+\sqrt{1+\varepsilon_2^2}}\right)^2\right\}\right.$$

$$\left.\left.- iD(\varepsilon_2, b_2)\right]\right\}e^{i\Omega\delta} \qquad (II.7)$$

$$\bar{w}_{rs} = \frac{\bar{\Gamma}}{4\pi\cdot\eta}\left[\bar{n}\left(\bar{k},W_1^{(g)}/W_2^{(g)}\right)\left(\frac{1}{v+1}\cdot\frac{1}{g_1\sqrt{1+g_1^2}} - \frac{1}{v-1}\cdot\frac{1}{g_2\sqrt{1+g_2^2}}\right)+\right.$$

$$+\left\{\frac{1}{v+1}\left[\frac{g_1}{\sqrt{1+g_1^2}} + e^{-ib_1g_1}\left\{1 - \frac{ib_1}{2}\log\left(\frac{g_1}{1+\sqrt{1+g_1^2}}\right)^2\right\} - iD(g_1,b_1)\right]\right.$$

$$\left.\left. - \frac{1}{v-1}\left[\frac{g_2}{\sqrt{1+g_2^2}} + e^{-ib_2g_2}\left\{1 - \frac{ib_2}{2}\log\left(\frac{g_2}{1+\sqrt{1+g_2^2}}\right)^2\right\} - iD(g_2,b_2)\right]\right\}e^{i\bar{k}\delta}\right] \qquad \text{(II.8)}$$

The following definitions pertain.

$$\left.\begin{aligned} \bar{k} &= k\,\frac{\eta}{b} \\ u &= x/\eta \quad ; \quad v = y/\eta \\ b_1 &= \bar{k}\,|v+1| \; ; \; b_2 = \bar{k}\,|v-1| \\ g_1 &= u/|v+1| \; ; \; g_2 = u/|v-1| \end{aligned}\right\} \qquad \text{(II.9)}$$

and δ is the distance from the bound vortex mid-span rearward to the trailing edge of the wing, divided by the local semi-chord. As shown in the main text, for the single-lifting-line approach $\delta = 3/2$ while for the double-lifting-line-theory, δ takes on the values $7/4$ and $3/4$ corresponding to the forward and rearward lifting-lines, respectively.

The principal function entering in (II.7), (II.8) is $D(g_1,b_1)$ and $D(g_2,b_2)$. Dropping the subscripts, it can be shown that

$$D(g,b) = e^{-ibg}\left[\left\{b(1+g^2)^{1/2} + b\bar{G}(b) - A(gb,b)\right\}\right.$$

$$\left. + i\left\{b\,\pi/2 + bF_I(b) + B(gb,b)\right\}\right] \qquad \text{(II.10)}$$

where

$$\left.\begin{aligned} F(b) &= \int_0^\infty e^{-i\lambda} \left\{ \frac{1}{b} + \frac{1}{\lambda} - \frac{\sqrt{\lambda^2 + b^2}}{\lambda b} \right\} d\lambda \\ &= F_R(b) + iF_I(b) \end{aligned}\right\} \qquad (II.11)$$

and

$$\left.\begin{aligned} \bar{G}(b) &= F_R(b) + \log 2b + \gamma - 1 \end{aligned}\right\}$$

In the latter equation, γ is the well-known Eulerian constant 0.5772 $\cdots\cdots$. Finally,

$$A(gb,b) = \int_0^{gb} \left\{ (1 - \cos\lambda) \sqrt{\lambda^2 + b^2}/\lambda \right\} d\lambda$$

$$B(gb,b) = \int_0^{gb} \left\{ \sin\lambda \sqrt{\lambda^2 + b^2}/\lambda \right\} d\lambda \qquad (II.12)$$

It is recognized that $F(b)$ is the complete Cicala function while the integrals in (II.12) are related to the incomplete Cicala function. Values of $F_R(b)$, $F_I(b)$ and $\bar{G}(b)$ have been tabulated by Luke and Hafford (Ref. 15). The integrals $A(gb,b)$ and $B(gb,b)$ are tabulated in a report by Bangler, Goland and Luke (Ref. 16). More recently, an extensive table of $F(b)$ has been prepared by the Harvard Computations Laboratory (Ref. 17). It is understood that they have also tabulated the integrals in (II.12) (or related ones).

Note that the function $B(g,b)$ contains no singularities. It is a two-parameter family. In view of the above tables, this function could be tabulated once and for all, so that for any wing configuration construction of the downwash coefficients would be an easy matter. It does not appear feasible to construct charts for the bracketed portion of $\bar{w}_{rs}$ directly as this is a three-parameter family.

APPENDIX III

A STEP BY STEP OUTLINE FOR THE COMPUTATION OF SPANWISE LIFT AND MOMENT DISTRIBUTIONS FOR OSCILLATING FINITE SPAN WINGS EMPLOYING THE SINGLE-LIFTING-LINE METHOD

In this appendix, an outline is presented for the steps required for the calculation of the spanwise lift and moment distributions for oscillating finite span wings using the single-lifting-line theory. The steps are as follows:

1. Replace the wing by a system of discrete horseshoe vortices as shown in Fig. 2. In the notation of this report, this fixes the values of η u, v, b_1, ϵ_1, etc. (See p. 59)

2. Choose k .

3. Compute $\bar{w}_{rs}$ as given by Eq. (II.9) for the values of r and s determined in Step 1. Note that subscript r refers to number of wing vortex while subscript s refers to position on the three-quarter chord line.

4. For the wing mode of interest, compute the total geometric downwash at the required three-quarter chord line stations. Note that for swept wings, in addition to contributions due to the wing bending and torsion mode shapes, a further contribution arises which is proportional to the spanwise change of the wing bending mode shape.

5. For each component of the geometric downwash derived in Step 4, determine the n values of $\bar{\Gamma}_r$ as defined by the set of n simultaneous equations, Eqs. (2.3).

6. Compute the spanwise distribution of circulatory lift as given by Eq. (2.5). Note that the present theory assumes that resultant lift of each wing section acts at the quarter chord. Thus the moment coefficients are the same as their two-dimensional counterparts.

7. Compute non-circulatory lift and moment distribution along the wing for each mode shape of interest employing two-dimensional strip theory. Note that the lift acts at the quarter chord.

8. Combine the circulatory and non-circulatory lift and moment contributions to formulate the total lift and moment.